UNIVERSITÀ DEGLI STUDI DI PADOVA
Dipartimento di Ingegneria Industriale DII
Corso di Laurea Magistrale in Ingegneria Meccanica

DEVELOPMENT AND INVESTIGATION OF A THREE-DIMENSIONAL VEHICLE MODEL FOR THE STUDY OF ADVANCED MAPS OF ACHIEVABLE PERFORMANCE (MAPS)

Relatore: Prof. Basilio Lenzo

Laureando: Giacomo Busato, 2083182

Anno Accademico 2024/2025

ABSTRACT

This work consists of the study and development of a three-dimensional vehicle model with 9 degrees of freedom, which is then exploited for the analysis of novel Maps of Achievable Performance (MAPs) within a purposely-developed Matlab tool. The vehicle model, which includes roll and pitch dynamics, is obtained with a state-space formulation, in which the load transfers play a critical role and represent four state variables. A novel expression for longitudinal load transfers under transient conditions is proposed. Importantly, roll and pitch moments are studied in two forms: the first includes the vertical forces acting at the contact patch of the tires, and the second includes the suspension reactions through stiffness and damping. The use of MAPs is a recently proposed approach to evaluate the handling of the vehicles. Yet, so far, MAPs have only been studied for planar vehicle models. Here, for the first time, the MAPs of a three-dimensional vehicle model are presented, including MAPs featuring roll and pitch angle, providing new insights in the field of vehicle dynamics theory.

SOMMARIO ESTESO

Le *Maps of Achievable Performance* (MAPs) rappresentano un nuovo strumento utile a indagare le caratteristiche di maneggevolezza di un veicolo, e sono una rappresentazione 2D di qualsiasi coppia di parametri collegati che caratterizzano lo stato di un veicolo a regime. Esse possono quindi fornire al lettore informazioni sulla performance ottenibile dal veicolo tramite un piano in cui vengono rappresentate le variabili di interesse, e in cui è possibile includere informazioni anche su una terza variabile tramite curve di livello. Nonostante siano uno strumento innovativo, esse possono essere ricavate per manovre standard già in uso nell'ambito della dinamica del veicolo: velocità costante con angolo di sterzo crescente e viceversa. Finora nella letteratura si trovano MAPs ricavate per modelli di veicolo sia a singola che a doppia traccia, ma sempre planari. In questa tesi l'obiettivo è ricavare delle MAPs per un modello di veicolo che includa la dinamica tridimensionale del veicolo, e quindi anche i movimenti di cassa di rollio e beccheggio. Per fare ciò è stato costruito un modello di veicolo che includa anche questi gradi di libertà, passando da un modello planare a uno tridimensionale, trascurando il movimento verticale del veicolo (scuotimento). Nel modello sono state incluse anche le dinamiche rotazionali delle ruote. Ne risulta quindi un modello a 9 gradi di libertà, in cui sono inclusi: velocità longitudinale e laterale, le tre rotazioni del veicolo (rollio, beccheggio, imbardata), le velocità di rotazione delle singole ruote. Il modello è stato implementato in un tool Matlab assieme a equazioni costitutive e di congruenza: le gomme sono state modellate secondo una Magic Formula semplificata (oppure con un modello Fiala), e nei carichi verticali agenti sulle ruote sono inclusi i trasferimenti di carico sia longitudinali che laterali. Le MAPs ottenute con questo strumento portano con sè per la prima volta la rappresentazione degli angoli di rollio e beccheggio, utili ad indagare la loro influenza sulle performance che un veicolo può esprimere.

CONTENTS

ABBREVIATIONS

CoG centre of gravity.

DAE Differential and Algebraic Equations.

DoF Degree of Freedom.

DT Double Track model.

EOM Equations of Motion.

MAP Map of Achievable Performance.

MF Magic Formula.

ODE Ordinary Differential Equation.

PC pitch center.

PI proportional-integrative controller.

RC roll center.

ST Single Track model.

VIP Vehicle Invariant Point.

NOMENCLATURE

δ wheel steering angle.

$\dot{\phi}$ roll velocity.

$\dot{\psi}$ yaw velocity (equivalent to r).

$\dot{\theta}$ pitch velocity.

ω_{ij} angular velocity of the ij wheel.

ϕ roll angle.

ψ yaw angle.

ρ_a air density.

θ pitch angle.

a_1 distance between front axle and CoG.

a_2 distance between rear axle and CoG.

A frontal area.

B stiffness factor in Magic Formula.

c_θ vehicle's pitch damping.

$c_{\phi 1}$ front axle's roll damping.

$c_{\phi 2}$ rear axle's roll damping.

C_{z1} front aerodynamic lift coefficient.

C_{z2} rear aerodynamic lift coefficient.

C_x aerodynamic drag coefficient.

C shape factor in Magic Formula.

D peak factor in Magic Formula.

d VIP height under the CoG.

E curvature factor in Magic Formula.

g gravitational acceleration.

h CoG height.

J_{xx} vehicle's roll inertia about CoG.

J_{xz} vehicle's cross moment of inertia.

J_{yy} vehicle's pitch inertia about CoG.

J_{zz} vehicle's yaw inertia about CoG.

J_w wheel spinning inertia.

k_θ vehicle's pitch stiffness.

$k_{\phi 1}$ front axle's roll stiffness.

$k_{\phi 2}$ rear axle's roll stiffness.

m vehicle mass.

q_1 front RC height.

q_2 rear RC height.

R_w wheel effective radius.

r yaw velocity.

t_1 front track.

t_2 rear track.

u longitudinal velocity.

v lateral velocity.

1 Introduction

1.1 Context

Road safety is a widespread topic that affects all people in their daily lives. In fact, it is not necessary to drive a car to be involved in a traffic accident, but passengers, pedestrians, and cyclists are also vulnerable. In the *Global status report on road safety 2023* ([1]) it is stated that approximately 1.19 million people die each year globally as a result of road traffic crashes, and more than half of all road traffic deaths are among vulnerable road users, including pedestrians, cyclists, and motorcyclists.
Another related topic is the advancement of autonomous driving. Many car manufacturers are investing in this technology to increase road safety, and the suggestion of connected mobility is so strong that a dedicated European alliance has been founded (ECAVA, European Connected and Autonomous Vehicle Alliance).
The science of vehicle dynamics plays an important role in this evolving technology, such as the reliability of software and sensors. It is important to note that the software of autonomous driving must know the vehicle capabilities, for example in emergency maneuvers. Thus, it is important that the car is aware of both its surroundings and its own *achievable performance*, in order to obtain vehicle maneuvering that is as faithful as possible to the command given by the software.
To improve the car's "self-awareness", it is possible to build a detailed vehicle model and to study its dynamic capabilities. In classic vehicle dynamics, there are some famous concepts that describe some features of the car, in particular the *understeer gradient*. It is a useful tool for identifying the *understeering* or *oversteering* behavior of a vehicle, but this concept is weak. In the past few years, a more general tool has been developed, and it can give information "at a glance": the *Maps of Achievable Performance (MAPs)* can give insights thanks to a 2D representation of many related vehicle parameters. A more detailed explanation is given in Chapter 5.
However, this tool has been developed for a pretty simple vehicle model, which does not include the three dimensional dynamics of a car. In general, 3D vehicle modeling is not a very common topic in the literature, and the sources are not always consistent with each other. In fact, some essential concepts useful to build a three-dimensional vehicle model could lead to different solutions depending on the engineer's interpretation, for example the coordinate systems, the location of the roll and pitch centers, the linearization of the equations, and so on.
In general, it would be remarkable to create an unambiguous 3D model which can be useful in both performance of the vehicles and the road safety.

1.2 Objectives

In this thesis, an in-plane model will be created firstly to obtain the MAPs related to a vehicle which is not affected by roll and pitch dynamics.
Then, the objective of this work is to develop a three-dimensional vehicle model which includes roll and pitch dynamics. The workflow starts from the mathematical description of the tire-road interaction, the kinematic relationship between the tires and the vehicle itself, and the equations of motion. This research will lead to a state-space formulation of the model with some novel features, which is then implemented in a Matlab tool. Different but equivalent formulations ensure the proper reliability of the model. It will be simulated to verify its functionality under transient conditions, and then used to build *advanced* MAPs that will include roll and pitch angles among the usual parameters.
Finally, the obtained MAPs will be studied to investigate how the dynamics of roll and pitch affect vehicle handling.
In addition, a literature review is carried out to compare different three-dimensional models.

2 VEHICLE DYNAMICS

The vehicle dynamics modeling is a widespread topic in literature, and it is possible to identify two main vehicle models:

- **single track model**: in this case, the vehicle is modeled as a two-wheel system, where the front and rear axles collapse into one wheel, which carries the characteristics of an equivalent axle.
- **double track model**: in this case, the vehicle is modeled with four wheels and it includes the constructive sizes of tracks which were not present in the single track model.

In this work, the focus is on the second one. Firstly, a planar model has been developed to verify the MAPs construction with literature materials [2]. Secondly, a three-dimensional model has been developed in order to obtain all-new MAPs which include roll and pitch dynamics.

2.1 Coordinate system

Before the illustration of the vehicle models, it is necessary to explain some assumptions made at the beginning of the work:

- the vehicle is assumed to be a rigid body;
- the unsprung masses are assumed negligible to the sprung mass, thus the entire mass is concentrated at the vehicle's CoG;
- the road is assumed to be flat and rigid;
- the vehicle is symmetrical about its longitudinal axis;
- the front steering is parallel;
- the vehicle has a rear-wheel drive and open differential;

The next step is the definition of a reference coordinate system. The vehicle equations will refer to this reference frame. It's possible to define two main coordinate system:

- ground-fixed coordinate system
- body-fixed coordinate system

2.1.1 Ground-fixed coordinate system

As the name suggests, this reference frame is fixed to the ground and it can be assumed as the "absolute" coordinate system $(S_0 = (x_0, y_0, z_0; O_0))$ for its inertial properties.
In this work, the *vehicle invariant point* (VIP) position describes the position of the whole vehicle,

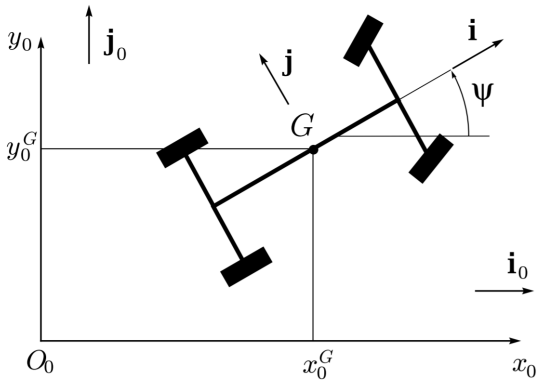

Figure 2.1: Ground-fixed coordinate system [3].

while the yaw angle (ψ) its orientation. The velocities are expressed in this coordinate system and then projected to the body-fixed one. A visual representation is in Fig. 2.1.
A remark on the position of CoG has to be done: in this work the goal is to build a three-dimensional model of the vehicle, including the roll and pitch motions. Thus, the CoG is no longer the centre of the moving reference frame since the sprung mass is not in a fixed orientation. It rotates around the VIP, a point which is not subject to the chassis' movements. Thus, it is a more reliable center for the moving reference frame.

2.1.2 Body-fixed coordinate system

A moving reference frame ($S = (x, y, z)$) is attached to the vehicle's body. According to the ISO convention, the coordinate system is defined as follows:

- x is the longitudinal axis, pointing in the forward direction and parallel to the road;
- y is the lateral axis, pointing in the left direction and parallel to the road;
- z is the vertical axis, pointing in the upward direction and perpendicular to the road.

The rotation about the three axes are the following:

- ϕ: roll angle, about the x-axis;
- θ: roll angle, about the y-axis;
- ψ: roll angle, about the z-axis;

A visual representation is in Fig. 2.2.

2.2 Theory fundamentals

Once the coordinate system has been defined, three sets of equations are needed to build a full vehicle dynamics model:

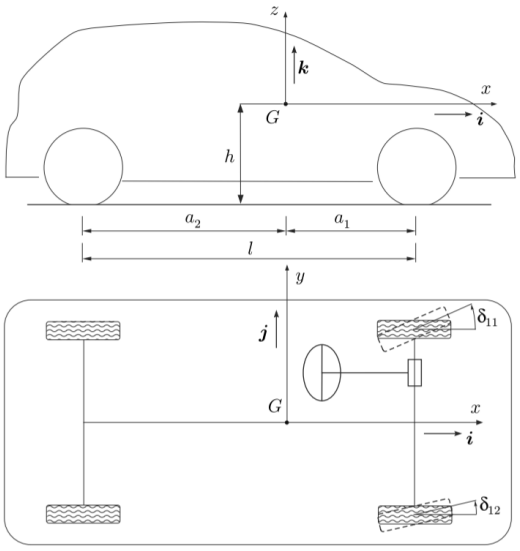

Figure 2.2: Body-fixed reference system [3].

- constitutive equations (tire model);
- congruence equations (kinematics);
- equilibrium equations (rigid body dynamics).

In this section, the first two sets are illustrated. In both planar and three-dimensional model, these features are expressed in the same way, while the equilibrium equations are different, including the vertical loads acting on the tires.

2.2.1 Congruence equations

Congruence equations represents the link between tire slips to the main vehicle kinematic quantities. In particular, tire slips depend on longitudinal and lateral velocities at the contact patch.
Starting from the velocity of the center of mass, G:

$$\mathbf{V_G} = u\mathbf{i} + v\mathbf{j} \tag{2.1}$$

and the rotation of the vehicle:

$$\mathbf{\Omega} = r\mathbf{k} \tag{2.2}$$

it is possible to obtain the velocity condition for any point P of the vehicle thanks to the known formulation for a rigid body:

$$\mathbf{V_P} = \mathbf{V_G} + \mathbf{\Omega} \times \mathbf{GP} \tag{2.3}$$

In particular, the components (u, v) are expressed in the body-fixed reference frame, while $\mathbf{V_G}$ is projected in the ground-fixed one. Moreover, the *yaw rate* r is considered positive if counterclockwise. Finally, it is possible to compute the velocity of any wheel contact patch P_{ij}, where the subscript i indicates the front axle ($i = 1$) or the rear axle ($i = 2$), while the j subscript indicates the left-hand side ($j = 1$) or the right-hand side ($j = 2$) of the vehicle.
The velocities of the tires at the contact patch are the following:

$$\mathbf{V_{11}} = (u - rt_1/2)\mathbf{i} + (v + ra_1)\mathbf{j} \tag{2.4}$$

$$\mathbf{V_{12}} = (u + rt_1/2)\mathbf{i} + (v + ra_1)\mathbf{j} \tag{2.5}$$

$$\mathbf{V_{21}} = (u - rt_2/2)\mathbf{i} + (v - ra_2)\mathbf{j} \tag{2.6}$$

$$\mathbf{V_{22}} = (u + rt_2/2)\mathbf{i} + (v - ra_2)\mathbf{j} \tag{2.7}$$

It is convenient to calculate the velocity components in each local tire frame:

$$V_{x,ij} = (\mathbf{V_{ij}} \cdot \mathbf{i}) \cos\delta + (\mathbf{V_{ij}} \cdot \mathbf{j}) \sin\delta \tag{2.8}$$

$$V_{y,ij} = -(\mathbf{V_{ij}} \cdot \mathbf{i}) \sin\delta + (\mathbf{V_{ij}} \cdot \mathbf{j}) \cos\delta \tag{2.9}$$

where δ is the steering angle. In this case, there is only front steering. The longitudinal velocities results in:

$$V_{x,11} = (u - rt_1/2)\cos\delta + (v + ra_1)\sin\delta \tag{2.10}$$

$$V_{x,12} = (u + rt_1/2)\cos\delta + (v + ra_1)\sin\delta \tag{2.11}$$

$$V_{x,21} = (u - rt_2/2) \tag{2.12}$$

$$V_{x,22} = (u + rt_2/2) \tag{2.13}$$

while the lateral velocities are:

$$V_{y,11} = -(u - rt_1/2)\sin\delta + (v + ra_1)\cos\delta \tag{2.14}$$

$$V_{x,12} = -(u + rt_1/2)\sin\delta + (v + ra_1)\cos\delta \tag{2.15}$$

$$V_{x,21} = (v - ra_2) \tag{2.16}$$

$$V_{x,22} = (v - ra_2) \tag{2.17}$$

Now that all components of the velocities are known, it is possible to define theoretical and practical slips.

Theoretical slips

The theoretical longitudinal slip is defined as:

$$\sigma_x = \frac{V_x - \omega R_w}{\omega R_w} \tag{2.18}$$

and applying to each tire:

$$\sigma_{x,11} = \frac{(u - rt_1/2)\cos\delta + (v + ra_1)\sin\delta - \omega_{11}R_w}{\omega_{11}R_w} \tag{2.19}$$

$$\sigma_{x,12} = \frac{(u + rt_1/2)\cos\delta + (v + ra_1)\sin\delta - \omega_{12}R_w}{\omega_{12}R_w} \tag{2.20}$$

$$\sigma_{x,12} = \frac{(u - rt_2/2) - \omega_{12}R_w}{\omega_{12}R_w} \tag{2.21}$$

$$\sigma_{x,22} = \frac{(u + rt_2/2) - \omega_{22}R_w}{\omega_{22}R_w} \tag{2.22}$$

The theoretical lateral slip is defined as:

$$\sigma_y = \frac{V_y}{\omega R_w} \tag{2.23}$$

and applying to each tire:

$$\sigma_{y,11} = \frac{-(u - rt_1/2)\sin\delta + (v + ra_1)\cos\delta}{\omega_{11}R_w} \tag{2.24}$$

$$\sigma_{y,12} = \frac{-(u + rt_1/2)\sin\delta + (v + ra_1)\cos\delta}{\omega_{12}R_w} \tag{2.25}$$

$$\sigma_{y,21} = \frac{v - ra_2}{\omega_{21}R_w} \tag{2.26}$$

$$\sigma_{y,22} = \frac{v - ra_2}{\omega_{22}R_w} \tag{2.27}$$

Practical slips

The slip ratio is defined as:

$$\kappa = \frac{\omega R_w - V_x}{V_x} \tag{2.28}$$

and applying to each tire:

$$\kappa_{11} = \frac{\omega_{11}R_w - (u - rt_1/2)\cos\delta - (v + ra_1)\sin\delta}{(u - rt_1/2)\cos\delta + (v + ra_1)\sin\delta} \tag{2.29}$$

$$\kappa_{12} = \frac{\omega_{12}R_w - (u + rt_1/2)\cos\delta - (v + ra_1)\sin\delta}{(u - rt_1/2)\cos\delta + (v + ra_1)\sin\delta} \tag{2.30}$$

$$\kappa_{12} = \frac{\omega_{12}R_w - (u - rt_2/2)}{(u - rt_2/2)} \tag{2.31}$$

$$\kappa_{12} = \frac{\omega_{12} R_w - (u + rt_2/2)}{(u + rt_2/2)} \tag{2.32}$$

The slip angle is defined as:

$$\alpha = \arctan\left(-\frac{V_y}{V_x}\right) \tag{2.33}$$

and applying to each tire:

$$\alpha_{11} = \arctan \frac{(u - rt_1/2)\sin\delta - (v + ra_1)\cos\delta}{(u - rt_1/2)\cos\delta + (v + ra_1)\sin\delta} \tag{2.34}$$

$$\alpha_{12} = \arctan \frac{(u + rt_1/2)\sin\delta - (v + ra_1)\cos\delta}{(u + rt_1/2)\cos\delta + (v + ra_1)\sin\delta} \tag{2.35}$$

$$\alpha_{21} = \arctan \frac{-(v - ra_2)}{(u - rt_2/2)} \tag{2.36}$$

$$\alpha_{22} = \arctan \frac{-(v - ra_2)}{(u + rt_2/2)} \tag{2.37}$$

It is possible to obtain the theoretical slips from the practical ones thanks to the following relationships:

$$\sigma_x = \frac{\kappa}{1 + \kappa} \tag{2.38}$$

$$\sigma_y = \frac{\tan\alpha}{1 + \kappa} \tag{2.39}$$

2.2.2 Constitutive equations

Constitutive equations are known as "tire models" as well, in fact they formalize the relationship between the forces generated by the tires and their deformations. Tires are considered generators of forces and moments, which are typically reported at the center of the tire contact patch. In particular, tires generate 3 forces (in x, y, z directions) and 3 moments around the three axis. In particular, the longitudinal force F_x is strictly related to the slip ratio κ, and the lateral force F_y to the slip angle α. In the "pure longitudinal" or "pure lateral" conditions, the tire is subject only to one of the slips. However, in real conditions, the combined slip reduces the peak of longitudinal and lateral force that the tire can generate. Therefore, in the following paragraphs this condition will be illustrated.
In this work three tire models can be used to run the simulations: the linear tire model, the Magic Formula, the Fiala tire model.

Linear tire model

This is the simplest model, in fact the relationship between the forces and the slips is linear. In particular, the slope is called "longitudinal stiffness" in the pure longitudinal slip, and "cornering stiffness" in the pure lateral slip. This model could fit the initial linear area of the plot force vs slip. Therefore, the force can be expressed as:

$$F = C_\sigma^F \sigma \tag{2.40}$$

where C is the generic stiffness and σ a generic slip:

$$C_\sigma^F = \left.\frac{\partial F}{\partial \sigma}\right|_{\sigma=0} \tag{2.41}$$

It is noticeable that this model is reliable for small slips only.

Magic Formula

This is a well-known model which offers a full description of the tire behavior, and it is based on a semi-empirical interpolation of experimental data. It uses a large number of coefficients, depending on the version. In this work, a simplified MF is used, including 4 parameters:

$$F = D\sin(C\arctan(B\sigma - E(B\sigma - \arctan B\sigma))) \tag{2.42}$$

The previous equation is the generic relationship between a force F and a slip σ, for example between F_x and κ.
The macro parameters are dependent on the vertical load acting on each tire:

- B: stiffness factor
$$B = \frac{a_3 \sin(2\arctan(F_z/a_4))}{C(a_1F_z + a_2)F_z} \tag{2.43}$$
- C: shape factor
$$C = 2 - \frac{2}{\pi}\arcsin y_m \tag{2.44}$$
- D: peak factor
$$D = (a_1F_z + a_2)F_z \tag{2.45}$$
- E: curvature factor
$$E = \frac{Bx_m - \tan(\frac{\pi}{2C})}{Bx_m - \arctan(Bx_m)} \tag{2.46}$$

where a_i, x_m, y_m are the micro parameters and F_z is the vertical load. It is noticeable that, in this case, the shape factor C is constant.

tanh-based tire model

This is a simpler model respect to Magic Formula. It is a tanh-based model function [4], where the generic relationship is:

$$F = F_z\mu\tanh\left(\frac{B_t}{\mu}\sigma\right) \tag{2.47}$$

with F_z the vertical load, μ the friction coefficient, B_t a tire parameter and σ a generic slip.
This model is less accurate respect to MF, in fact it doesn't show the tire saturation.

Combined slip

As said before, during driving the tire is subject to combined slip most of the time, which means that, for example, it generates both lateral and longitudinal force. It is possible to describe this condition with weighing functions, or with a simpler combination of the tire slips. In this work, the combined slip is defined as follows:

$$\sigma = \sqrt{\sigma_x^2 + \sigma_y^2} \tag{2.48}$$

i.e. the total slip due to the theoretical slips. Then, the forces are distributed linearly:

$$F_x = \frac{\sigma_x}{\sigma} F_t \tag{2.49}$$

$$F_y = \frac{\sigma_y}{\sigma} F_t \tag{2.50}$$

where F_t is the total force generated by the tire. For example, introducing (2.48) in (2.42), the total force due to the combined slip is calculated. Then, to obtain the longitudinal and lateral forces, (2.49) and (2.50) must be used. In Fig. 2.3 it is noticeable the decrease of force in combined condition.

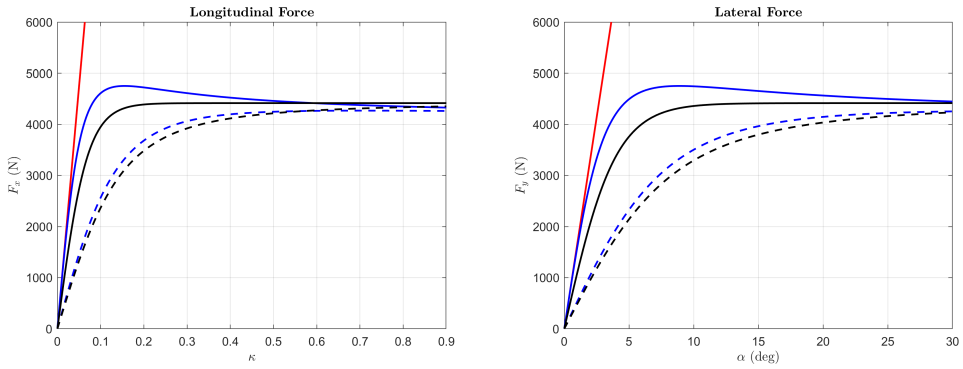

Figure 2.3: Forces vs slips. In red the linear model, in solid blue the MF model, in solid black the tanh-based model. The dashed lines represents the combined slip in MF and tanh-based.

2.2.3 Other forces acting on the vehicle

It is necessary to point out all the forces acting on the vehicle to have a comprehensive and functional model. In the previous sections, the road-tire interaction was described. However, it is clear that it is dependent on the vertical load acting on the tire. Therefore, the forces aligned in z-axis will affect the equilibrium equations. In addition, the tires' longitudinal forces are not the only forces in this direction. In this work, 4 types of forces are considered:

- gravitational force (weight)
- aerodynamic force (both downforce and drag)

- road-tire friction force (illustrated in Sec. 2.2.2)
- road-tire vertical force

Gravitational force

The weight of the vehicle is directed in the negative z-axis:

$$\mathbf{W} = -mg\mathbf{k} \tag{2.51}$$

Aerodynamic forces

The interaction between the car and the air generates two forces: the *drag* and the *lift*, described by the following equations.

$$F_D = \frac{1}{2}\rho C_x A u^2 \tag{2.52}$$

$$F_1^a = \frac{1}{2}\rho C_{z1} A u^2 \tag{2.53}$$

$$F_2^a = \frac{1}{2}\rho C_{z2} A u^2 \tag{2.54}$$

The lift force can be computed for the front and rear axles separately. It can be positive or negative, depending on the lift coefficient C_{zi} sign. On the opposite, the drag force is always negative and thus opposite to the vehicle motion.

Road-tire vertical force

This category depend on gravitational force, aerodynamic lift, longitudinal and lateral load transfers. A full insight is presented in both planar model and three-dimensional model in the following chapters.

3 IN-PLANE DT MODEL

In this chapter the derivation of dynamics equation for a planar double track model is presented. In particular, the calculation of the total road-tire vertical forces is reported. Then, the derivation of the equations of motion is obtained following the Newton method. Finally, a DAE system is builded in order to solve the differential equations together with some algebraic equations. The solution includes many vehicle parameters useful to build MAPs.
The planar model is characterized by 3 DoFs: $x = [u, v, r]^T$, and the input parameters are (u_0, δ), i.e. the test longitudinal velocity and the steering angle.

3.1 Hypotheses

In this work the state variables are named according to the classical nomenclature:

- u: longitudinal velocity
- v: lateral velocity
- r: yaw rate (also identified by the symbol $\dot{\psi}$)

The model considered in this work is characterized by the following hypotheses:

- double track vehicle, with parallel steering, rear wheel drive and open differential. Front and rear tracks are equal;
- in-plane motion and forces: the road is considered flat and tire deflections or suspension movements are not taken in account, i.e. roll and pitch dynamics are neglected;
- simplified Pacejka tire model;
- load transfers and vertical forces (i.e. aero) are considered in order to calculate the vertical load on each tire;
- steady state condition: $\dot{u} = \dot{v} = \dot{r} = 0$.

In Fig. 3.1 is reported a double track model. The longitudinal and lateral velocities are aligned with the body fixed reference frame along x and y direction, respectively. The yaw rate r is about the vertical axis z.

3.2 Congruence and constitutive equations

The two set of equations for slips and tire model are illustrated in Chapter 2. All the equations reported are used in this in-plane model, in particular the Magic Formula is implemented.

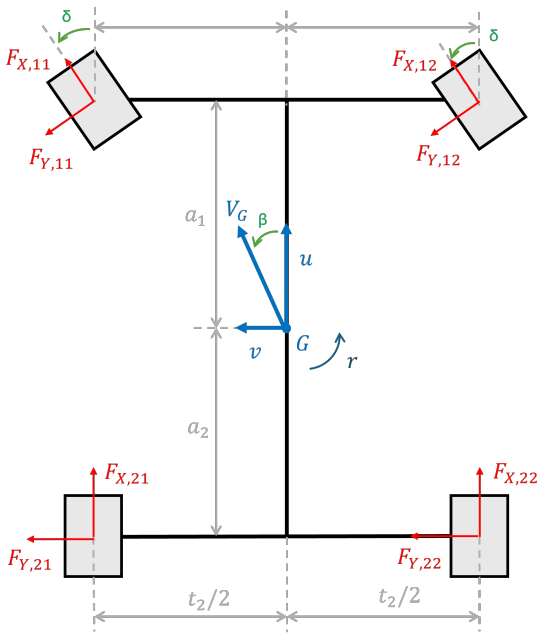

Figure 3.1: Outline of planar double track model.

3.3 Road-tire vertical forces

Each tire is subject to a vertical force given by four contributions:

- static load
- aerodynamic downforce
- longitudinal load transfer
- lateral load transfer

3.3.1 Static load

The vertical force acting on each axle when the vehicle is in standstill condition is:

$$F_1^{z0} = mg\frac{a_2}{a_1 + a_2} \tag{3.1}$$

$$F_2^{z0} = mg\frac{a_1}{a_1 + a_2} \tag{3.2}$$

Considering a single tire, the previous equations must be halved.

3.3.2 Aerodynamic load

The downforce contribution is given by:

$$F_1^a = \frac{1}{2}\rho C_{z1} A u^2 \tag{3.3}$$

$$F_2^a = \frac{1}{2}\rho C_{z2} A u^2 \tag{3.4}$$

Also in this case the contribution to a single tire is the half of the previous equations.

3.3.3 Longitudinal load transfer

The longitudinal acceleration is:

$$a_x = \dot{u} - vr = -vr \tag{3.5}$$

remembering that there is the hypotheses of steady state condition.
The longitudinal load transfers are:

$$\Delta F_z^x = -ma_x \frac{h}{a_1 + a_2} = -m(-vr)\frac{h}{a_1 + a_2} \tag{3.6}$$

In this case, the half of the previous expression must be added to each front tire, and subtracted from each rear tire.

3.3.4 Lateral load transfer

The lateral acceleration is:

$$a_y = \dot{v} + ur = ur \tag{3.7}$$

It is possible to compute the total lateral force acting on each axle ([3]):

$$F_{y,1} = \frac{ma_y a_2 + (J_z\dot{r} - N_x)}{a_1 + a_2} = \frac{mura_2 - N_x}{a_1 + a_2} \tag{3.8}$$

$$F_{y,2} = \frac{ma_y a_1 - (J_z\dot{r} - N_x)}{a_1 + a_2} = \frac{mura_1 + N_x}{a_1 + a_2} \tag{3.9}$$

since in steady state $\dot{r} = 0$. The momentum N_x is the torque about the z-axis due to the different longitudinal forces generated by the tires in the vehicle reference frame:

$$N_x = (\Delta F_{x,1} + \Delta F_{x,2})t = \left(\frac{(F_{y,11} - F_{y,12})\sin\delta + (F_{x,12} - F_{x,11})\cos\delta}{2} + \frac{F_{x,22} - F_{x,21}}{2}\right) t \tag{3.10}$$

At this point it is possible to obtain the expression for the lateral load transfers:

$$\Delta F_{z,1} = \frac{1}{t}\left((F_{y,1} + F_{y,2})\frac{k_{\phi 1}}{k_{\phi 1} + k_{\phi 2}}(h - d) + F_{y,1}q_1\right) \tag{3.11}$$

$$\Delta F_{z,2} = \frac{1}{t}\left((F_{y,1} + F_{y,2})\frac{k_{\phi 2}}{k_{\phi 1} + k_{\phi 2}}(h - d) + F_{y,2}q_2\right) \tag{3.12}$$

where d is the roll center height located under the CoG. In this case the load transfer on each axle must be added on the outside and subtracted from the inside. Since the convention used implies that the car is taking a left turn, the right side is more loaded than the left one.

3.3.5 Total vertical load on each tire

Composing all the contributions:

$$F_{z,11} = \frac{F_1^{z0}}{2} + \frac{F_1^a}{2} + \frac{\Delta F_z^x}{2} - \Delta F_{z,1} \tag{3.13}$$

$$F_{z,12} = \frac{F_1^{z0}}{2} + \frac{F_1^a}{2} + \frac{\Delta F_z^x}{2} + \Delta F_{z,1} \tag{3.14}$$

$$F_{z,21} = \frac{F_2^{z0}}{2} + \frac{F_2^a}{2} - \frac{\Delta F_z^x}{2} - \Delta F_{z,2} \tag{3.15}$$

$$F_{z,22} = \frac{F_2^{z0}}{2} + \frac{F_2^a}{2} - \frac{\Delta F_z^x}{2} + \Delta F_{z,2} \tag{3.16}$$

3.4 Equilibrium equations

The third set of equations is obtained considering rigid body dynamics. Therefore, considering a planar motion, three differential equations describe the vehicle motion with the three state variables (u, v, r). The classical force and torque equations are:

$$\begin{aligned} m\mathbf{a_G} &= \mathbf{F} \\ \dot{\mathbf{K}}_{\mathbf{G}}^{\mathbf{r}} &= \mathbf{M_G} \end{aligned} \tag{3.17}$$

where m is the total vehicle mass, $\mathbf{a_G}$ is the acceleration of its CoG, $\mathbf{F}$ is the resultant of all forces applied to the vehicle body, $\dot{\mathbf{K}}_{\mathbf{G}}^{\mathbf{r}}$ is the rate of change of the angular momentum of the vehicle body with respect to CoG, and $\mathbf{M_G}$ is the global moment of all forces with respect to CoG. Three equations are obtained: longitudinal equilibrium, lateral equilibrium, rotational equilibrium.

$$m(\dot{u} - vr) = F_{x,tot} \tag{3.18}$$

$$m(\dot{v} + ur) = F_{y,tot} \tag{3.19}$$

$$J_z\dot{r} = N \tag{3.20}$$

where

$$F_{x,tot} = F_{x,21} + F_{x,22} + (F_{x,11} + F_{x,12})\cos\delta - (F_{y,11} + F_{y,12})\sin\delta - F_{drag} \tag{3.21}$$

$$F_{y,tot} = (F_{y,11} + F_{y,12})\cos\delta + (F_{x,11} + F_{x,12})\sin\delta + F_{y,21} + F_{y,22} \tag{3.22}$$

$$\begin{aligned} N =& [(F_{y,11} + F_{y,12})\cos\delta + (F_{x,11} + F_{x,12})\sin\delta]a_1 - (F_{y,21} + F_{y,22})a_2 + \\ &+ [(F_{y,11} - F_{y,12})\sin\delta + (F_{x,22} - F_{x,21}) + (F_{x,12} - F_{x,11})\cos\delta]\frac{t}{2} \end{aligned} \tag{3.23}$$

In addition, despite the vertical displacement is discarded, it is remarkable to verify the vertical equilibrium:

$$0 = -mg - F_1^a - F_2^a + F_{z,11} + F_{z,12} + F_{z,21} + F_{z,22} \tag{3.24}$$

3.5 Algebraic equations

In the previous section the equilibrium equations were presented. In particular, the differential equations (3.18),(3.19),(3.20) can be solved to obtain the solution (u, v, r). However, it is noticeable that there are other three unknown variables in the many equations illustrated: the wheel angular velocities of the rear tires (the front tires' slip ratio is 0, thanks to the hypotheses of rear wheel drive) and the torque N_x.
It is necessary to impose three constraints, which will lead to a unique solution. Therefore, a DAE system will be composed. The hypotheses reported in 3.1 can impose two constraints, and the third algebraic equation derives from the definition of N_x.

3.5.1 Longitudinal velocity

In 3.1 it is stated that the longitudinal velocity is imposed. Considering a test speed named u_0, the first constraint is:

$$u = u_0 \tag{3.25}$$

It is possible to impose this condition thanks to the steady state condition and the input parameters. It is possible to run two different analysis:

- fixed u and slowly increasing δ;
- fixed δ and slowly increasing u.

In both cases, each pair (u, δ) is studied in steady state condition, allowing to use the constraint in (3.25).

3.5.2 Open differential

An open differential lead to equal forces on both the wheels connected to it. Thus, this hypothesis is useful to impose a zero difference between the longitudinal force generated by the rear wheels:

$$\Delta F_{x,2} = F_{x,21} - F_{x,22} = 0 \tag{3.26}$$

3.5.3 N_x definition

Introducing the (3.10) to the set of equations, the system is made of 6 equations with 6 unknown variables. It is useful to express this equation as follows:

$$N_x - (\Delta F_{x,1} + \Delta F_{x,2})t = 0 \tag{3.27}$$

3.6 DAE system

At this point it is possible to compose the DAE system which can be solved numerically:

$$\begin{aligned} m(\dot{u} - vr) &= F_{x,tot} \\ m(\dot{v} + ur) &= F_{y,tot} \\ J_z\dot{r} &= N \\ u &= u_0 \\ F_{x,21} - F_{x,22} &= 0 \\ N_x - (\Delta F_{x,1} + \Delta F_{x,2})t &= 0 \end{aligned} \tag{3.28}$$

4 3D VEHICLE MODEL

This chapter describes the construction of a three-dimensional vehicle model with 9 DoFs, which include the roll and pitch dynamics. The following pages will illustrate many aspects on which to focus attention, since the spatial dynamics include CoG movements, the identification of centers of instantaneous rotation, and different load transfers.
In this case, the equations of motion are assisted by some additional differential equations in order to compose a state-space formulation. Thus, the state variables are 16 in total.

4.1 Hypotheses

This model has 9 degrees of freedom:

- u, longitudinal velocity;
- v, lateral velocity;
- ϕ, roll angle;
- θ, pitch angle;
- $\dot{\psi}$, yaw velocity (can be expressed as r);
- ω_{ij}, 4 wheels angular velocity.

The input parameters are as usual (u, δ), i.e. longitudinal velocity and steering angle. The model considered in this work is characterized by the following hypotheses:

- double track vehicle, with parallel steering, rear wheel drive and open differential. Front and rear tracks are equal;
- spatial motion;
- simplified Pacejka tire model;
- load transfers and vertical forces (i.e. aero) are considered in order to calculate the vertical load on each tire;

In this case, a ODE simulation is carried out to verify the functionality of the model, making an analysis of the state variables signals. Therefore, the same model is used to obtain the MAPs in steady state conditions.
The vehicle parameters are reported in Table 4.1.

Parameter	Symbol (unit)	Value
Fixed parameters		
Distance of front axle from CoG	$a_1\,(m)$	1.125
Distance of rear axle from CoG	$a_1\,(m)$	1.375
Front track	$t_1\,(m)$	1.6
Rear track	$t_2\,(m)$	1.6
Front roll centre height	$q_1\,(m)$	0.05
Rear roll centre height	$q_2\,(m)$	0.1
CoG height	$h\,(m)$	0.55
Inertial parameters		
Vehicle mass	$m\,(kg)$	2000
Moment of inertia w.r.t. x axis	$J_{xx}\,(kg\,m^2)$	800
Moment of inertia w.r.t. y axis	$J_{yy}\,(kg\,m^2)$	2500
Moment of inertia w.r.t. z axis	$J_{zz}\,(kg\,m^2)$	2846
Cross moment of inertia w.r.t. x-z axis	$J_{xz}\,(kg\,m^2)$	100
Tyre parameters		
Wheel radius	$R_w\,(m)$	0.25
Rolling inertia	$J_w\,(kg\,m^2)$	1.3
MF micro parameter	$a_1\,(kN^{-1})$	-0.05
MF micro parameter	$a_2\,(-)$	1.3
MF micro parameter	$a_3\,(kN/rad)$	120
MF micro parameter	$a_4\,(kN)$	4
MF micro parameter	$x_m\,(-)$	0.15
MF micro parameter	$y_m\,(-)$	0.87
Suspension parameters		
Front roll stiffness	$k_{\phi 1}\,(Nm/rad)$	40000
Rear roll stiffness	$k_{\phi 2}\,(Nm/rad)$	42000
Front roll damping	$c_{\phi 1}\,(Nms/rad)$	10000
Rear roll damping	$c_{\phi 2}\,(Nms/rad)$	10000
Global pitch stiffness	$k_\theta\,(Nm/rad)$	80000
Global pitch damping	$c_\theta\,(Nms/rad)$	50000
Aerodynamic parameters		
Drag coefficient	$C_x\,(-)$	0.35
Front lift coefficient	$C_{z1}\,(-)$	-0.077
Rear lift coefficient	$C_{z2}\,(-)$	0.077
Frontal area	$A\,(m^2)$	2
Air density	$\rho_a\,(kg/m^3)$	1.225

Table 4.1: Vehicle Parameters.

4.2 Coordinate systems

When dealing with roll and pitch in a vehicle system, the problem become three-dimensional. In this case, it is convenient to define unambiguously the orientation of the vehicle body, rather than its position. In fact, the body rotations ϕ, roll angle, and θ, pitch angle, causes some movements of the CoG respect to the wheels, which are not affected by these effects (at least in their position, it is known that the roll motion has influence on the camber variation of the wheels). Thus it's possible to say that the wheel position is unchanged respect to a ground-fixed reference frame, while the CoG position is subject to roll and pitch motions and it is not fixed.
Then it is important to define the orientation of the vehicle body with respect to a ground-fixed reference frame, which will be called S_0, as in 2.1.1. Since the vehicle is considered a rigid body, it is possible to define its orientation by means of three elemental rotations in a definite order. In this case, the sequence is *yaw(ψ)-pitch(θ)-roll(ϕ)*. Since there are three rotations, four coordinate systems are generated. Each system shares one axis with the precedent one and another different axis with the next one ([3], Chapter 9):

$$(\mathbf{i_0}, \mathbf{j_0}, \mathbf{k_0}) \xrightarrow[\mathbf{k_0}=\mathbf{k_1}]{\psi} (\mathbf{i_1}, \mathbf{j_1}, \mathbf{k_1}) \xrightarrow[\mathbf{j_1}=\mathbf{j_2}]{\theta} (\mathbf{i_2}, \mathbf{j_2}, \mathbf{k_2}) \xrightarrow[\mathbf{i_2}=\mathbf{i_3}]{\phi} (\mathbf{i_3}, \mathbf{j_3}, \mathbf{k_3}) \tag{4.1}$$

The final system S_3 is the vehicle-fixed reference frame, in which $\mathbf{k_3}$ is orthogonal to the road and $\mathbf{i_3}$ is parallel to the road when the vehicle is at rest. A visual representation is in Fig. 4.1.

4.2.1 Vehicle Invariant Point (VIP)

This section illustrates a crucial concept for this work. In the previous pages, it was reported that the CoG is not fixed with respect to the vehicle position in a three-dimensional system. Thus, it is necessary to find a point which is fixed respect to the wheels, i.e. follows the vehicle motion, and is not subject to roll and pitch. This point coincides with the origin O_1 of the reference system S_1, which is subject to yaw but not to pitch and roll. Considering Fig. 4.2, the no-roll center Q is located on the line connecting the front and rear no-roll centers, and it is right under the CoG. Recalling the reference system S_3, it is known the direction $\mathbf{i_3}$ about which the vehicle rolls, but it is not defined a particular axis about which the vehicle rolls. The point searched is almost unaffected by roll and pitch, and thus it remains centered with respect to the tire contact patches. Since the front and rear no-roll centers are also called *track invariant point* ([3], Chapter 9), it is clear that the desired point is located between them, and in the reference configuration it coincides with Q. Thus it is called *vehicle invariant point*, and it is located in the middle of the vehicle even when it rolls.
In this work, it is assumed that the VIP is also the no-pitch center, i.e. the point about which the vehicle pitches. As for the no-roll centers, its position is defined by the suspension design, which is not object of study in this work. However, an example is reported in Fig. 4.3. The green lines identify the instantaneous center of rotation between the front unsprung mass and the sprung mass. Similar for the orange lines in the rear axle. The tire contact patch is the rotation center between the unsprung mass and the ground. Therefore, connecting the contact patch center

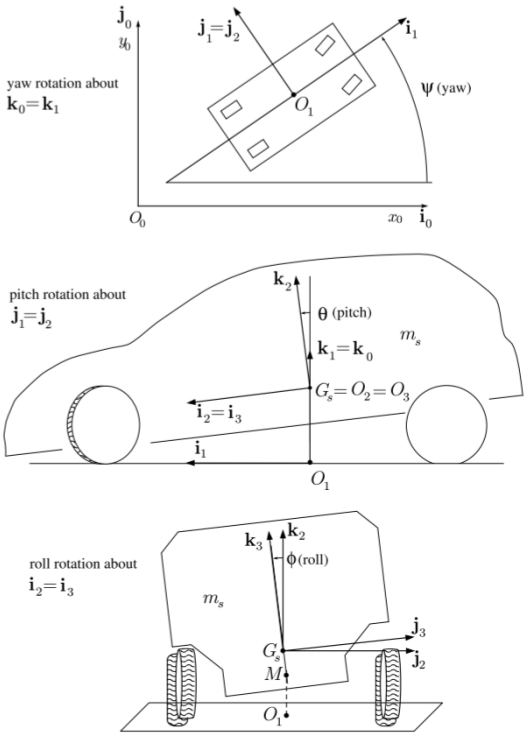

Figure 4.1: Definition of the various reference systems, with the rotation sequence yaw-pitch-roll [3].

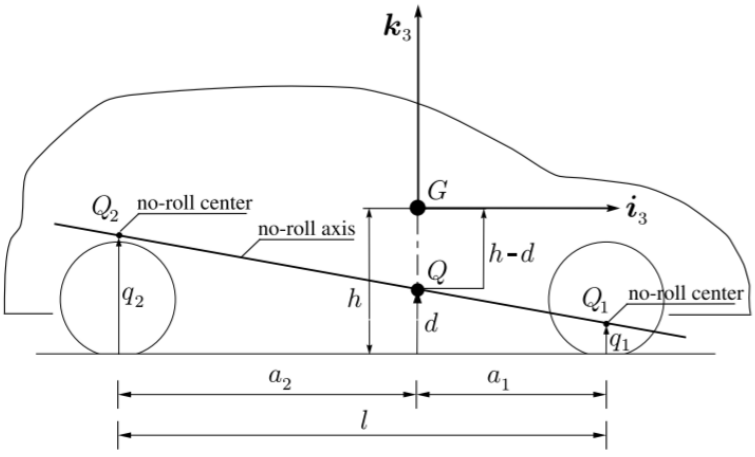

Figure 4.2: Side view of the vehicle with no-roll centers highlighted [3].

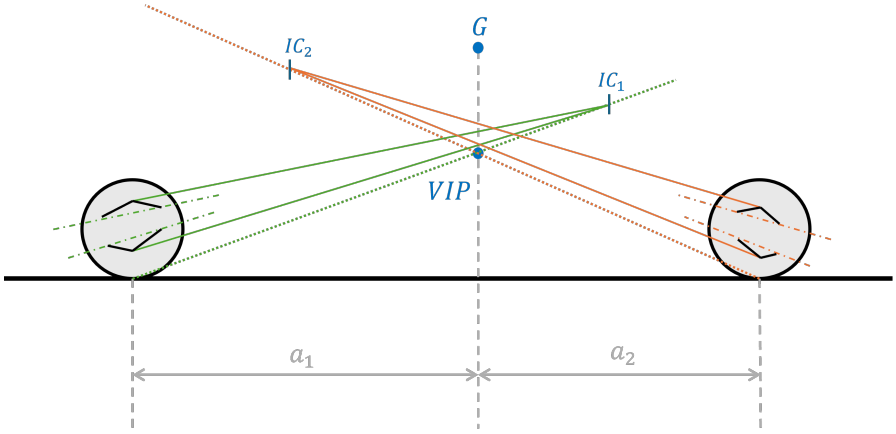

Figure 4.3: Construction of no-pitch center for double-wishbone suspensions.

with the IC_i, it is known thanks to the Aronhold-Kennedy theorem that the instantaneous center of rotation between the sprung mass and the ground, i.e. the no-pitch center, is located on the dashed lines. Composing the two axles, the point about which the car pitches is defined. As said before, in this work it is assumed that the no-pitch center height is equal to the no-roll center one, combining the two points in one, which is the VIP.

4.3 Roll and pitch motions

At this point, it is necessary to consider the different expression of the yaw moment about the z-axis centered in CoG. In fact, if the moved CoG is called G', the arms of the forces with respect to G' are no longer the half-track and a_1, a_2, depending on the direction considered, but they are affected by roll and pitch. On the other hand, the yaw moment about VIP remains equal to 3.23, since the VIP is fixed and right under the CoG when at rest. Then, two new torque equations must be introduced: one about the x-axis and one about the y-axis. Also in these cases, the expression about G' are different respect to the ones about VIP. In the next sections, the various cases are presented.

4.3.1 External torques respect to G'

The point G' in the reference system S_1 has the following coordinates, which correspond to the vector connecting VIP to G'. It is named MG:

$$\mathbf{MG} = \begin{bmatrix} (h-d)\theta \\ -(h-d)\phi \\ (h-d) \end{bmatrix} \tag{4.2}$$

It is noticeable that the vertical coordinate is not affected by the two angles. In fact, assuming small angles, it is possible to consider the height of G' equal to the height h of the CoG at rest. It

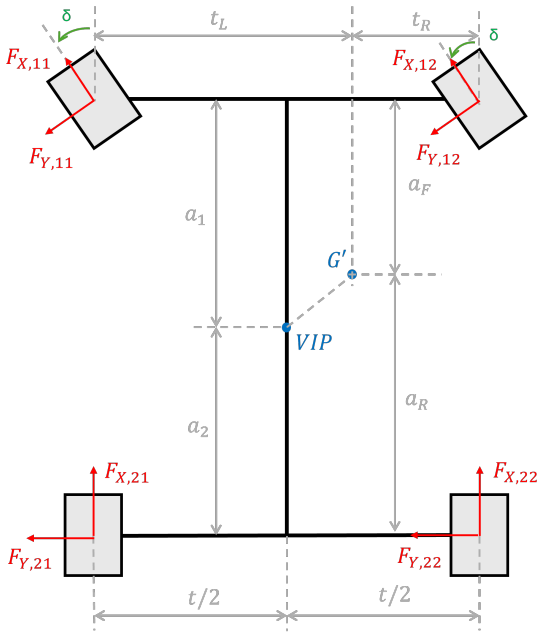

Figure 4.4: Top view of the vehicle model.

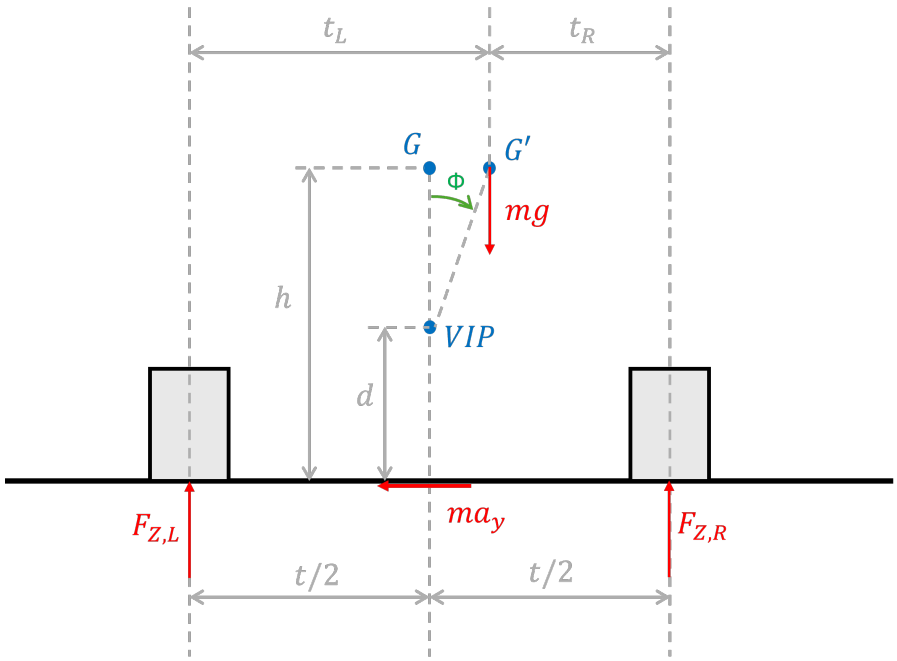

Figure 4.5: Rear view of the vehicle model. $F_{Z,L}$ is the sum of the vertical forces on the left-hand side, while $F_{Z,R}$ is the sum on the right-hand side.

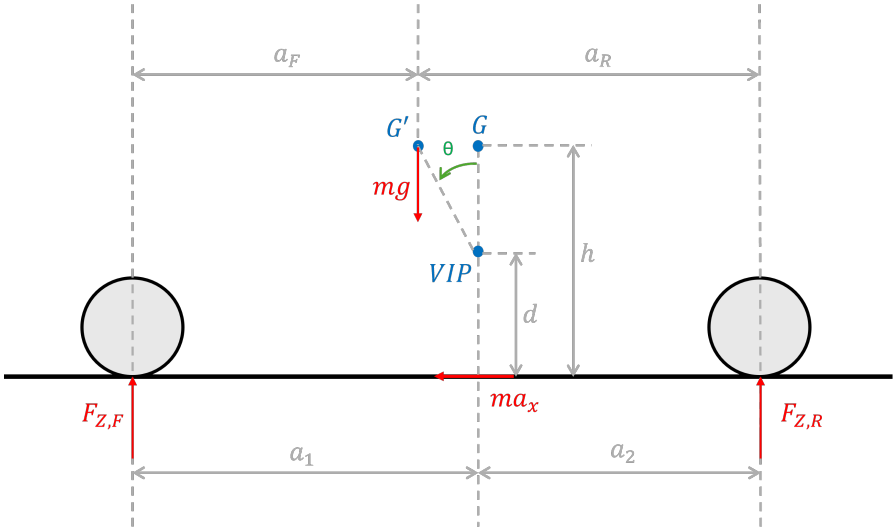

Figure 4.6: Side view of the vehicle model. $F_{Z,F}$ is the sum of the vertical forces on the front axle, while $F_{Z,R}$ is the sum on the rear axle.

is reported in S_1 because the EOM will be written in this reference frame, which is attached to the vehicle and it is convenient for the expression of external forces and moments, as done in 3.4. Considering Figg. 4.4,4.5,4.6, the following parameters are defined:

$$t_L = \frac{t}{2} + (h-d)\phi \tag{4.3}$$

$$t_R = \frac{t}{2} - (h-d)\phi \tag{4.4}$$

$$a_F = a_1 - (h-d)\theta \tag{4.5}$$

$$a_R = a_2 + (h-d)\theta \tag{4.6}$$

Yaw moment

Writing the torque equation respect to G' and considering Fig. 4.4, the following expression is obtained:

$$\begin{aligned} N_{G'} = [(F_{y,11} + F_{y,12})\cos\delta + (F_{x,11} + F_{x,12})\sin\delta](a_1 - (h-d)\theta) + \\ -(F_{y,21} + F_{y,22})(a_2 + (h-d)\theta) + \\ +(F_{x,12}\cos\delta - F_{y,12}\sin\delta + F_{x,22})(\frac{t}{2} - (h-d)\phi) + \\ +(F_{y,11}\sin\delta - F_{x,11}\cos\delta - F_{x,21})(\frac{t}{2} + (h-d)\phi) \end{aligned} \tag{4.7}$$

Considering 3.23, and knowing that $F_{y,tot} = ma_y$ and $F_{x,tot} = ma_x$, after some calculations it is possible to relate the yaw moment respect to G' with the 3.23:

$$N_{G'} = N - m(h-d)(\theta a_y + \phi a_x) \tag{4.8}$$

with a_x, a_y not yet defined.

Roll moment

The external torque about the longitudinal axis and respect to G' reads:

$$L_{G'} = (F_{z,11} + F_{z,21})(\frac{t}{2} + (h-d)\phi) - (F_{z,12} + F_{z,22})(\frac{t}{2} - (h-d)\phi) + ma_y h \tag{4.9}$$

The term ma_y represent the total lateral force generated at the contact patch between the 4 tires and the road.
The roll angle sign is determined by the right-hand rule, considering the x-axis entering the sheet. In Fig. 4.5 the car is taking a left turn.

Pitch moment

The external torque about the lateral axis and respect to G' reads:

$$M_{G'} = -(F_{z,11} + F_{z,12} - F_1^a)(a_1 - (h-d)\theta) + (F_{z,21} + F_{z,22} - F_2^a)(a_2 + (h-d)\theta) - ma_x h \tag{4.10}$$

The term ma_x represent the total longitudinal force generated at the contact patch between the 4 tires and the road.
The pitch angle sign is determined by the right-hand rule, considering the y-axis pointing forward (front axle is on the left).

External moments due to stiffness and damping

It is also possible to compute the external moments considering the stiffness and damping features of the suspensions. This method is reserved to roll and pitch moments. The global roll stiffness and roll damping coefficients are given by the sum of the two axles' stiffness and damping:

$$k_\phi = k_{\phi 1} + k_{\phi 2} \tag{4.11}$$

$$c_\phi = c_{\phi 1} + c_{\phi 2} \tag{4.12}$$

The pitch parameters are global and are not split into front and rear axle.
Therefore, it is possible to express the two torques by inserting the complete expressions of $F_{z,ij}$ in 4.9,4.10 and knowing that $F_{y,1}q_1 + F_{y,2}q_2 = F_{y,tot}d$:

$$L_{G'} = -k_\phi \phi - c_\phi \dot{\phi} + ma_y(h-d) + mg(h-d)\phi \tag{4.13}$$

$$M_{G'} = -k_\theta \theta - c_\theta \dot{\theta} - ma_x(h-d) + mg(h-d)\theta \tag{4.14}$$

4.3.2 External torques respect to VIP

When considering the VIP as reference point, the torque expressions are a little simpler, due to the position fixed in the middle plane of the car and not subject to roll and pitch motions. The Figg. 4.4,4.5,4.6 are considered again to write the following paragraphs. It is remarkable that the gravitational force is now considered due to the moved configuration of CoG.

Yaw moment

In this case, the expressions obtained is equivalent to 3.23:

$$\begin{aligned} N_{VIP} = N = [(F_{y,11} + F_{y,12})\cos\delta + (F_{x,11} + F_{x,12})\sin\delta]a_1 - (F_{y,21} + F_{y,22})a_2 + \\ + [(F_{y,11} - F_{y,12})\sin\delta + (F_{x,22} - F_{x,21}) + (F_{x,12} - F_{x,11})\cos\delta]\frac{t}{2} \end{aligned} \tag{4.15}$$

Roll moment

As said before, since the gravitational force is eccentric respect to the VIP, it causes a torque about this point. The external moment becomes:

$$L_{VIP} = (F_{z,11} + F_{z,21} - F_{z,12} - F_{z,22})\frac{t}{2} + ma_y d + mg(h-d)\phi \tag{4.16}$$

It should be noted that the total lateral force ma_y has a different arm respect to 4.9.

Pitch moment

The same considerations made for the roll moment can be done here. The external moment is the following:

$$M_{VIP} = -(F_{z,11} + F_{z,12} - F_1^a)a_1 + (F_{z,21} + F_{z,22} - F_2^a)a_2 - ma_x d + mg(h-d)\theta \tag{4.17}$$

External moments due to stiffness and damping

As in the case of the equation referred to G', it is possible to express the external moments with the suspensions' forces:

$$L_{VIP} = -k_\phi\phi - c_\phi\dot{\phi} + mg(h-d)\phi \tag{4.18}$$

$$M_{VIP} = -k_\theta\theta - c_\theta\dot{\theta} + mg(h-d)\theta \tag{4.19}$$

4.4 Load transfers

This section is a crucial point in model construction. As reported in 4.1, the hypothesis of steady state condition is initially discarded. Considering the transient conditions, it is not possible to compute the load transfer in the same way as 3.6,3.11,3.12, in fact, these equations refer to steady state conditions. Load transfers are affected by longitudinal and lateral acceleration, which are affected by the time derivatives of the state variables listed in 4.1. Therefore it is convenient to define the load transfers acting on each tire as state variables [5], in order to avoid an algebraic loop issue. This solution leads to four additional differential equations, one for each tire, in which a "rate of change" over a time τ of the load transfer is modeled. The time step τ is the same as the simulation options. The differential equations are expressed as:

$$\Delta\dot{F}_{z,ij} = \frac{\Delta\tilde{F}_{z,ij} - \Delta F_{z,ij}}{\tau} \tag{4.20}$$

with $\Delta F_{z,ij}$ the state variable and

$$\Delta \tilde{F}_{z,ij} = \pm \frac{\Delta F_z^x}{2} \pm \Delta F_{z,i}^y \tag{4.21}$$

i.e. the sum of longitudinal and lateral load transfers. It is remarkable to focus on their expressions, especially on longitudinal load transfer. In fact, an alternative version is proposed in the following paragraph. The convention used to impose the sign of the load transfers is the same used in the planar model:

$$\begin{aligned}
\Delta \tilde{F}_{z,11} &= +\frac{\Delta F_z^x}{2} - \Delta F_{z,1}^y \\
\Delta \tilde{F}_{z,12} &= +\frac{\Delta F_z^x}{2} + \Delta F_{z,1}^y \\
\Delta \tilde{F}_{z,21} &= -\frac{\Delta F_z^x}{2} - \Delta F_{z,2}^y \\
\Delta \tilde{F}_{z,22} &= -\frac{\Delta F_z^x}{2} + \Delta F_{z,2}^y
\end{aligned} \tag{4.22}$$

Finally, it can be remarked the computation of the total vertical load acting on each tire:

$$F_{z,11} = \frac{F_1^{z0}}{2} + \frac{F_1^a}{2} + \Delta F_{z,11} \tag{4.23}$$

$$F_{z,12} = \frac{F_1^{z0}}{2} + \frac{F_1^a}{2} + \Delta F_{z,12} \tag{4.24}$$

$$F_{z,21} = \frac{F_2^{z0}}{2} + \frac{F_2^a}{2} + \Delta F_{z,21} \tag{4.25}$$

$$F_{z,22} = \frac{F_2^{z0}}{2} + \frac{F_2^a}{2} + \Delta F_{z,22} \tag{4.26}$$

It is noticeable that the state variable $\Delta F_{z,ij}$ is always added to the sum, since the sign of load transfer is considered in 4.22.

4.4.1 Longitudinal load transfer

In transient condition, the formulation is the following ([3], Chapter 9):

$$\Delta F_z^x = -\frac{m a_x h + J_y \ddot{\theta}}{a_1 + a_2} \tag{4.27}$$

where it is useful to remember that $m a_x = F_{x,tot}$.
In this work an alternative expression is obtained by imposing the equality between the external torque about y-axis, i.e. the pitch moment, in 4.17 and in 4.19. The method consists in the following steps:

1. impose 4.17=4.19
2. substitute the terms $F_{z,ij}$ with the complete expressions
3. set ΔF_z^x as the unknown variable

4. solve for ΔF_z^x

The result is the following alternative expression for longitudinal load transfer:

$$\Delta F_z^x = -\frac{-k_\theta \theta - c_\theta \dot{\theta} + m a_x d}{a_1 + a_2} \tag{4.28}$$

which is similar to the lateral load transfers reported in the next paragraph.

4.4.2 Lateral load transfers

In transient conditions, the formulation is the following ([3], Chapter 9):

$$\Delta F_{z,i}^y = \frac{F_{y,i} d_i + k_{\phi,i} \phi + c_{\phi,i} \dot{\phi}}{t_i} \tag{4.29}$$

where i refers to the axles, as always.

4.5 Wheel dynamics

The wheels' angular velocities are 4 DoFs of the model. Therefore, their dynamics represents four differential equations. The equilibrium of a wheel subject to a torque is as follows:

$$\dot{\omega}_{ij} = \frac{T_i - F_{x,ij} R_w}{J_w} \tag{4.30}$$

where T_i is the axle's torque, R_w is the tire radius, J_w is the wheel rolling inertia. It should be noted that for front wheels $T_1 = 0$ since the vehicle is a rear wheel drive. Therefore, the free rolling condition of front wheels has to be verified after the simulation run.
The simulations are carried out at fixed longitudinal velocity and steering angle. However, since there is a transient before the equilibrium of the steady state condition, a torque controller has to be implemented, in order to give the right amount of torque to satisfy the longitudinal equilibrium. This problem is solved with a Proportional-Integrative (PI) controller.

4.5.1 PI controller

A PI controller is a feedback-based control loop mechanism which can react to an error by tending to the null value. It receives the current value as input and the error is the difference between the target value and the current one. The reaction can be tuned by means of coefficients. In a PI controller there are two terms:

- **proportional term**: the error signal is multiplied by a constant K_P
- **integral term**: this term accounts for the past values of the error over time and multiply its integral by a constant K_I

Considering a generic signal $s(t)$, the expression is the following:

$$s(t) = K_P e(t) + K_I \int_0^t e(\tau)\, d\tau \tag{4.31}$$

with $e(t)$ the error.
In this work, the target value is represented by the longitudinal velocity u_0, and the input parameter is the state variable u.
The output parameter is the torque transmitted to the rear wheels. Therefore, its expression is:

$$T_2(t) = K_P(u_0 - u(t)) + K_I \int_0^t (u_0 - u(\tau))\, d\tau \tag{4.32}$$

However, the integral term is not known. To solve this problem, it is considered a state variable of the system, in fact an additional differential equation can be added to the set:

$$\dot{int}(e) = e \tag{4.33}$$

In fact, the derivative of the error integral is the error itself.
It is possible to generalize 4.32 introducing the torque distribution parameter between the front and rear axle TD_i:

$$TD_1 = \frac{T_1}{T_1 + T_2} \tag{4.34}$$

$$TD_2 = \frac{T_2}{T_1 + T_2} \tag{4.35}$$

In this work, $TD_1 = 0$ and $TD_2 = 1$. The final expression for the torques are obtained:

$$T_1 = TD_1(K_P(u_0 - u(t)) + K_I int(e)) \tag{4.36}$$

$$T_2 = TD_2(K_P(u_0 - u(t)) + K_I int(e)) \tag{4.37}$$

After some tuning, the gain values are the following: $K_P = 100, K_I = 50$.

4.6 Equations of motion

In this section, the body accelerations are finally reported. Roll and pitch motions affect the translational equilibrium, and the fundamental formula for rigid body can be used:

$$\mathbf{a_G} = \mathbf{a_{VIP}} + \dot{\mathbf{\Omega}} \times \mathbf{MG} + \mathbf{\Omega} \times (\mathbf{\Omega} \times \mathbf{MG}) \tag{4.38}$$

where 4.2 is used, and the angular velocity in the vehicle-fixed reference frame is ([3], Chapter 9):

$$\mathbf{\Omega} = (\dot{\phi} - \dot{\psi}\theta)\mathbf{i_3} + (\dot{\theta} + \dot{\psi}\phi)\mathbf{j_3} + \dot{\psi}\mathbf{k_3} \tag{4.39}$$

After the derivation reported in Chapter 9 of [3], longitudinal and lateral accelerations must be updated:

$$a_x = \dot{u} - vr + (h - d)\ddot{\theta} \tag{4.40}$$

$$a_y = \dot{v} + ur - (h-d)\ddot{\phi} \tag{4.41}$$

Using the Newton method reported in 3.17, the second equation must be updated if written with respect to VIP with the generalized form:

$$\dot{\mathbf{K}}_G^r + \mathbf{MG} \times m\mathbf{a_G} = \mathbf{M}_{VIP} \tag{4.42}$$

The derivation of the first term of the left-hand side is reported in Chapter 9 of [3], while the calculation of the second term is illustrated here. It is useful to recall 4.2 and specify the acceleration vector:

$$\mathbf{a_G} = \begin{bmatrix} \dot{u} - vr + (h-d)\ddot{\theta} \\ \dot{v} + ur - (h-d)\ddot{\phi} \\ 0 \end{bmatrix} = \begin{bmatrix} a_x \\ a_y \\ 0 \end{bmatrix} \tag{4.43}$$

Therefore, the vector product is:

$$\mathbf{MG} \times m\mathbf{a_G} = m \begin{bmatrix} (h-d)^2\ddot{\phi} - (h-d)(\dot{v} + ur) \\ (h-d)^2\ddot{\theta} + (h-d)(\dot{u} - vr) \\ (h-d)(\theta a_y + \phi a_x) \end{bmatrix} \tag{4.44}$$

At this point it is possible to define the equilibrium equations in both references, i.e. G' and VIP.

4.6.1 EOM - G' reference

The equations of motion written in G' reference follow the classical equations 3.17, and they are illustrated here:

$$\begin{aligned} m(\dot{u} - vr + (h-d)\ddot{\theta}) &= F_{x,tot} \\ m(\dot{v} + ur - (h-d)\ddot{\phi}) &= F_{y,tot} \\ J_x\ddot{\phi} - J_{xz}\dot{r} &= L_{G'} \\ J_y\ddot{\theta} &= M_{G'} \\ J_z\dot{r} - J_{xz}\ddot{\phi} &= N_{G'} \end{aligned} \tag{4.45}$$

where the right-hand side terms can be found in the previous sections.

4.6.2 EOM - VIP reference

The equations of motion written in VIP reference follow the first of 3.17 and 4.42:

$$\begin{aligned} m(\dot{u} - vr + (h-d)\ddot{\theta}) &= F_{x,tot} \\ m(\dot{v} + ur - (h-d)\ddot{\phi}) &= F_{y,tot} \\ (J_x + m(h-d)^2)\ddot{\phi} - J_{xz}\dot{r} - m(h-d)(\dot{v} + ur) &= L_{VIP} \\ (J_y + m(h-d)^2)\ddot{\theta} + m(h-d)(\dot{u} - vr) &= M_{VIP} \\ J_z\dot{r} - J_{xz}\ddot{\phi} + m(h-d)(\theta a_y + \phi a_x) &= N \end{aligned} \tag{4.46}$$

where N_{VIP} is written as N since they are equal. Also in this case, the right-hand side terms can be found in the previous sections.

4.7 State-space formulation and simulations

The final step is the state-space formulation, where the state vector is:

$$\mathbf{x} = \begin{bmatrix} u & v & r & \phi & \theta & \dot{\phi} & \dot{\theta} & \Delta F_{z,11} & \Delta F_{z,12} & \Delta F_{z,21} \\ \Delta F_{z,22} & \omega_{11} & \omega_{12} & \omega_{21} & \omega_{22} & int(e) & & & & \end{bmatrix}^T \tag{4.47}$$

It should be noted that two auxiliary state variables are added: $\dot{\phi}$ and $\dot{\theta}$. In fact, two auxiliary equations are necessary to keep the first order system: $\dot{\phi} = d\phi/dt$ and $\dot{\theta} = d\theta/dt$. Therefore, the terms $\ddot{\phi}, \ddot{\theta}$ are the first derivative of $\dot{\phi}, \dot{\theta}$ and not the second derivative of ϕ, θ.
To keep the consistency with the previous sections, the state-space formulation is illustrated for both the references (G' and VIP). However, the equilibrium equations reported in 4.45 and 4.46 represent the only difference between the two formulations.

4.7.1 G' reference

Composing 4.45, the auxiliary equations, the 4.20 for each wheel, the 4.30 for each wheel and 4.33, the state-space model is:

$$\begin{aligned}
m(\dot{u} - vr + (h-d)\ddot{\theta}) &= F_{x,tot} \\
m(\dot{v} + ur - (h-d)\ddot{\phi}) &= F_{y,tot} \\
J_x\ddot{\phi} - J_{xz}\dot{r} &= L_{G'} \\
J_y\ddot{\theta} &= M_{G'} \\
J_z\dot{r} - J_{xz}\ddot{\phi} &= N_{G'} \\
\dot{\phi} &= \dot{\phi} \\
\dot{\theta} &= \dot{\theta} \\
\Delta\dot{F}_{z,11} &= \frac{\Delta\tilde{F}_{z,11} - \Delta F_{z,11}}{\tau} \\
\Delta\dot{F}_{z,12} &= \frac{\Delta\tilde{F}_{z,12} - \Delta F_{z,12}}{\tau} \\
\Delta\dot{F}_{z,21} &= \frac{\Delta\tilde{F}_{z,21} - \Delta F_{z,21}}{\tau} \\
\Delta\dot{F}_{z,22} &= \frac{\Delta\tilde{F}_{z,22} - \Delta F_{z,22}}{\tau} \\
\dot{\omega}_{11} &= \frac{T_1 - F_{x,11}R_w}{J_w} \\
\dot{\omega}_{12} &= \frac{T_1 - F_{x,12}R_w}{J_w} \\
\dot{\omega}_{21} &= \frac{T_2 - F_{x,21}R_w}{J_w} \\
\dot{\omega}_{22} &= \frac{T_2 - F_{x,22}R_w}{J_w} \\
\dot{int}(e) &= e
\end{aligned} \tag{4.48}$$

4.7.2 VIP reference

Doing the same as the previous section, the model referred to the VIP is different for the first five equations:

$$
\begin{aligned}
m(\dot{u} - vr + (h-d)\ddot{\theta}) &= F_{x,tot} \\
m(\dot{v} + ur - (h-d)\ddot{\phi}) &= F_{y,tot} \\
(J_x + m(h-d)^2)\ddot{\phi} - J_{xz}\dot{r} - m(h-d)(\dot{v} + ur) &= L_{VIP} \\
(J_y + m(h-d)^2)\ddot{\theta} + m(h-d)(\dot{u} - vr) &= M_{VIP} \\
J_z\dot{r} - J_{xz}\ddot{\phi} + m(h-d)(\theta a_y + \phi a_x) &= N \\
\dot{\phi} &= \dot{\phi} \\
\dot{\theta} &= \dot{\theta} \\
\Delta\dot{F}_{z,11} &= \frac{\Delta\tilde{F}_{z,11} - \Delta F_{z,11}}{\tau} \\
\Delta\dot{F}_{z,12} &= \frac{\Delta\tilde{F}_{z,12} - \Delta F_{z,12}}{\tau} \\
\Delta\dot{F}_{z,21} &= \frac{\Delta\tilde{F}_{z,21} - \Delta F_{z,21}}{\tau} \\
\Delta\dot{F}_{z,22} &= \frac{\Delta\tilde{F}_{z,22} - \Delta F_{z,22}}{\tau} \\
\dot{\omega}_{11} &= \frac{T_1 - F_{x,11}R_w}{J_w} \\
\dot{\omega}_{12} &= \frac{T_1 - F_{x,12}R_w}{J_w} \\
\dot{\omega}_{21} &= \frac{T_2 - F_{x,21}R_w}{J_w} \\
\dot{\omega}_{22} &= \frac{T_2 - F_{x,22}R_w}{J_w} \\
\dot{int}(e) &= e
\end{aligned}
\tag{4.49}
$$

4.7.3 Simulation results

The state-space model illustrated in the previous pages is useful for running simulations with an ODE solver. In particular, the test is a really simple maneuver with fixed (u_0, δ). In the following graphs, a simulation with $u_0 = 10m/s$ and $\delta = 15\,\mathrm{deg}$ is reported. The solid blue lines represent the G'-referred model, while the dashed red lines represent the VIP-referred model. The initial conditions are pretty simple: all state variables are set null for $t = 0$, except for the longitudinal velocity and the wheels' angular velocities:

- $u(0) = u_0 - 5\ m/s$
- $\omega_{ij}(0) = (u_0/R_w)/0.9812$, i.e. a little amount of slip ratio is imposed.

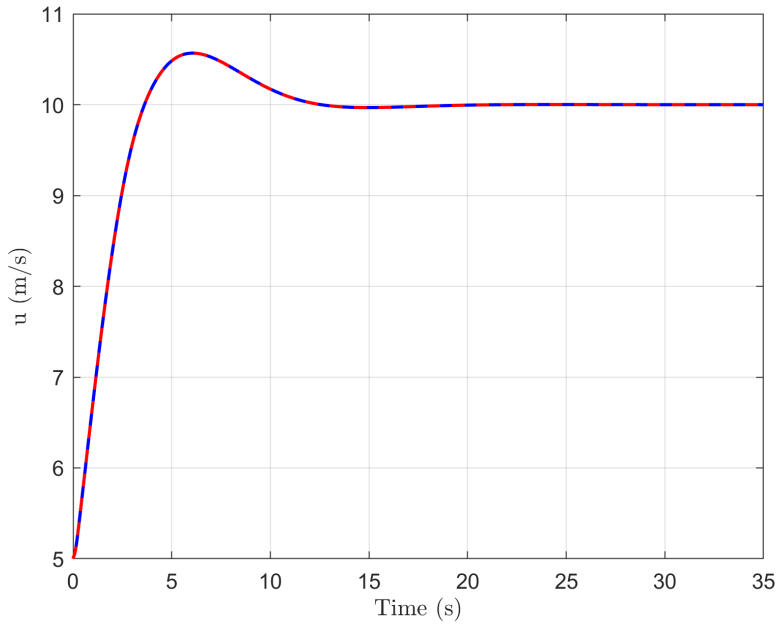

Figure 4.7: Longitudinal velocity signal.

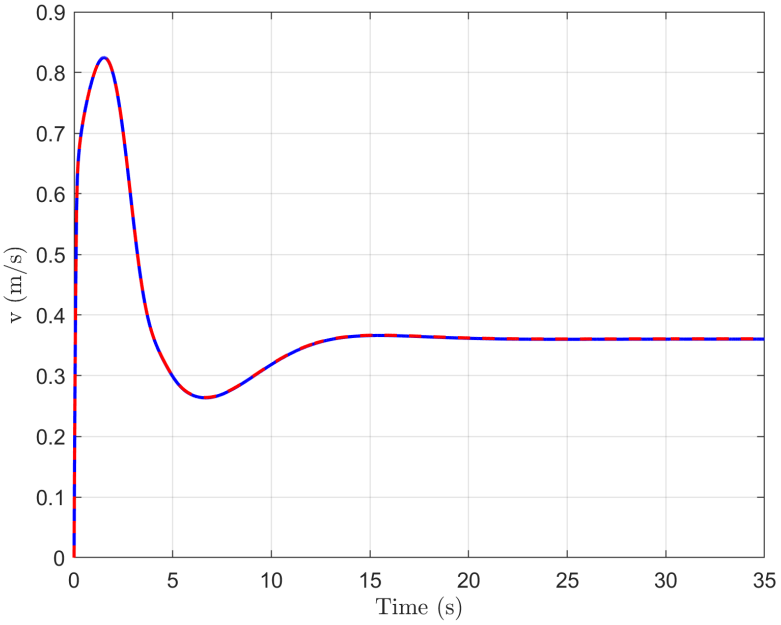

Figure 4.8: Lateral velocity signal.

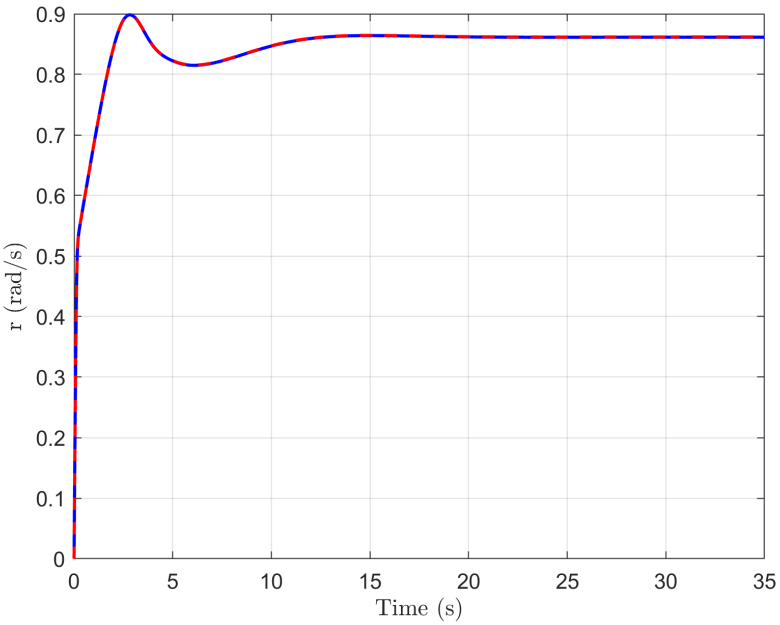

Figure 4.9: Yaw velocity signal.

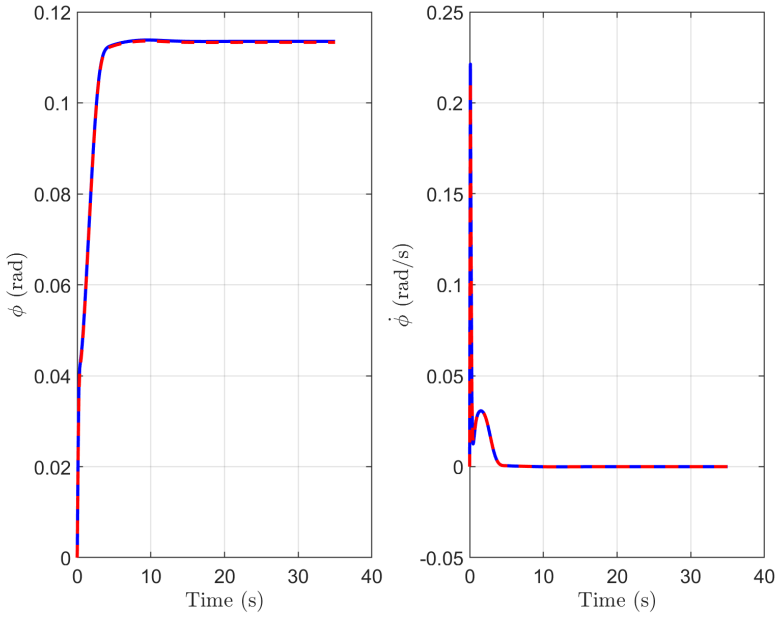

Figure 4.10: Roll angle and roll velocity signals.

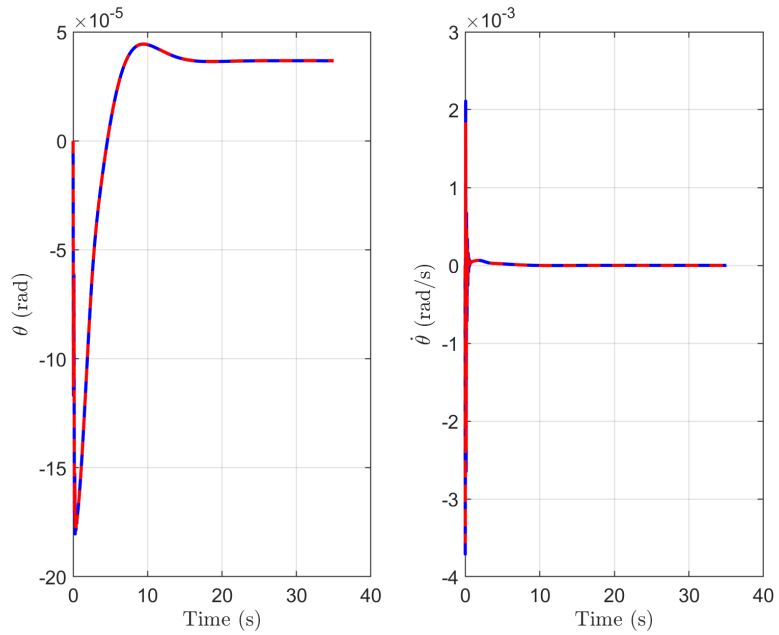

Figure 4.11: Pitch angle and pitch velocity signals.

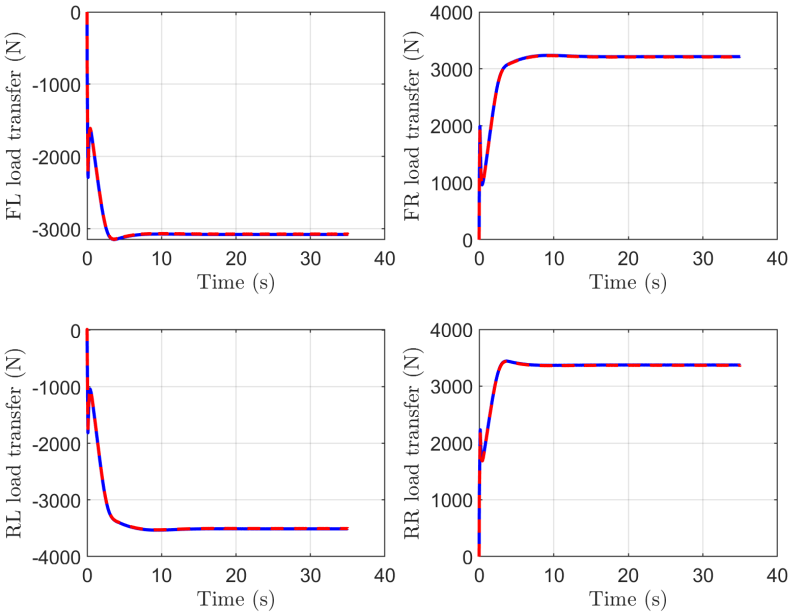

Figure 4.12: Load transfers signals.

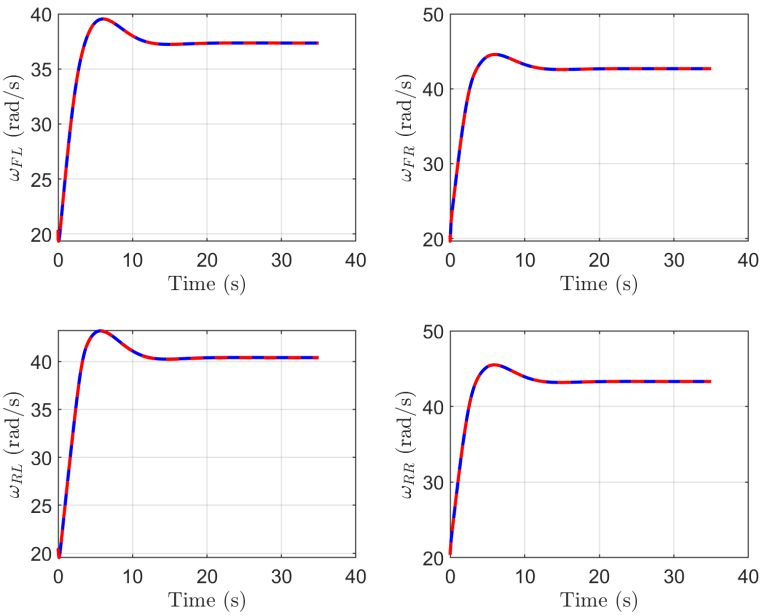

Figure 4.13: Wheels' angular velocities signals.

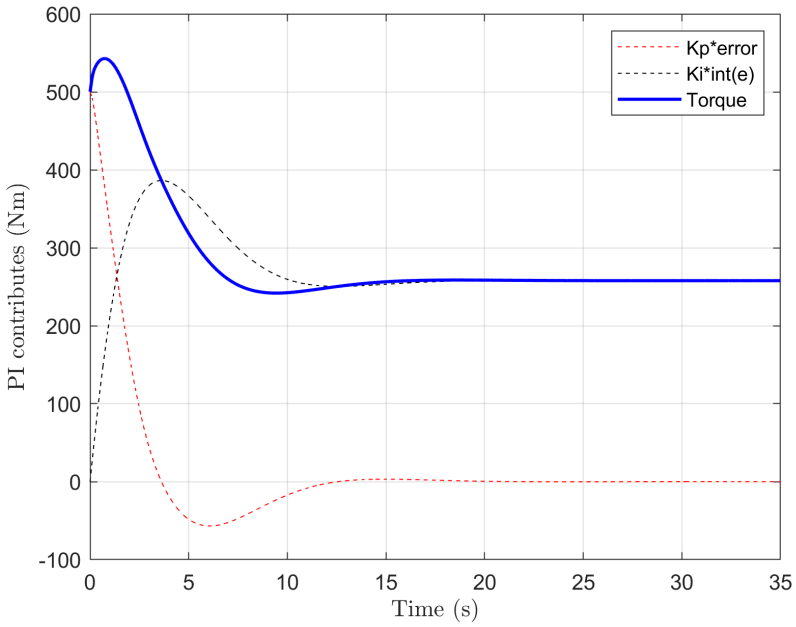

Figure 4.14: PI controller contributes and output torque signals.

The PI control is noticeable on the longitudinal velocity u. The roll and pitch dynamics are characterized by an initial transient condition where the velocities are not null, while at the equilibrium they are zero. This leads to non-null values of roll and pitch angles.
The signs and values of load transfers are as expected: negative on the left-hand side and positive on the right-hand side, and with higher absolute values on the rear axle. This matches the convention of left turn and the roll stiffness distribution of the vehicle, which is higher at the rear axle. The wheels' angular velocities are lower at the front axle due to the free rolling condition, and the inside wheel, i.e. the front left one, is slower than the outside wheel. On the other hand, the velocities are higher at the rear axle, due to the tractive role.
This simple analysis confirms the functionality of the model, which can be implemented to obtain the MAPs. It is also noticeable the almost perfect superimposing between the two different models: despite the different formulation, they are identical.

4.8 Literature review

In this section a literature review is carried out to compare the model that has been developed in this thesis with other works. The main differences can be found in the equations of motion and in the calculation of load transfers. In particular, the EOM can be different due to the choice of the reference systems and the location of the roll center (RC) and pitch center (PC).

In [6] a "Derivation of a Six Degrees-of-Freedom Ground-Vehicle Model for Automotive Applications" is illustrated. It is similar to the derivation reported in Chapter 9 of [3], which is the basis of this thesis. However, the equations of motion reported in this technical report refer to the CoG, and are derived in a body-fixed reference frame with the same characteristics featured in 2.1.2. The sequence of three elementary rotations is *yaw-pitch-roll*, as in 4.2. Moving on with the EOM, the first focus is on the translational equilibriums. In this thesis, the assumption of small roll and pitch angles is made. Thus, $\sin\phi \approx \phi, \sin\theta \approx \theta$ and $\cos\phi, \cos\theta \approx 1$. Moreover, the quadratic terms and the mixed derivative or angle products are negligible. Applying this simplification to equations (13),(14),(15),(16),(17) in [6], the result is the following:

$$\begin{aligned} \dot{u} &= v\dot{\psi} - h\ddot{\theta} + F_x/m \\ \dot{v} &= -u\dot{\psi} + h\ddot{\phi} + F_y/m \\ J_{xx}\ddot{\phi} &= -k_\phi\phi - c_\phi\dot{\phi} + mgh\phi + ma_y h \\ J_{yy}\ddot{\theta} &= -k_\theta\theta - c_\theta\dot{\theta} + mgh\theta - ma_x h \\ J_{zz}\ddot{\psi} &= N - h(ma_x\phi + ma_y\theta) \end{aligned} \tag{4.50}$$

The first difference from 4.45 is the lack of terms with the cross product of inertia J_{xz} in the third and fifth equations, and this is due to a simplification in [6], where the inertia tensor is considered diagonal. Then, in the first two equations, the only difference is the term h, which also in the reference is the height of CoG above ground at rest. In this thesis, the roll and pitch accelerations are multiplied by the term $(h - d)$. This difference is also noticeable in the external

torques of the rotational equations. Therefore, the two models are really similar, except for the difference between h and $(h-d)$. However, in road vehicles, the height d of the RC is very low. In [6] the heights of the RC and PC are not defined. In addition, the wheel dynamics are modeled in the same way as in this thesis. Lastly, load transfers are similar to 4.28,4.29, except for the missing terms $ma_x d$ and $ma_y d$. Taking into account this difference and the equations in 4.50, it is possible to hypothesize that RC and PC are on the ground.

In [7] a 14 DoFs full vehicle model is reported. Here, there is the separation between the sprung and unsprung masses. The first non-negligible difference with the model presented in this thesis is the CoG acceleration. In fact, a_x and a_y are considered as in the planar model. This is an ambiguous interpretation of a three-dimensional vehicle model, in fact roll acceleration and pitch acceleration contributes are neglected. Then, the pitch center is located on the ground, and the equilibrium is calculated as follows:

$$J_{yy}\ddot{\theta} = m_s a_x h + m_s g h\theta - k_\theta \theta - c_\theta \dot{\theta} \tag{4.51}$$

This equation could appear similar to the fourth of 4.45 with $M_{G'}$ from 4.14. However, the left-hand side needs more attention, since the pitch inertia J_{yy} is usually calculated with reference to CoG, and in this case the rotation is considered about a different point. Secondly, on the right-hand side the inertial term has an opposite sign with respect to this work (see 4.14). Moving on to the roll equilibrium, the equation is written with respect to the roll center:

$$(J_x + m_s(h-d)^2)\ddot{\phi} = m_s a_y (h-d)\cos\phi + m_s g(h-d)\sin\phi - k_\phi \phi - c_\phi \dot{\phi} \tag{4.52}$$

The comparison with the third equation in 4.46 with L_{VIP} from 4.18 suggests two differences: on the left side the term $J_{xz}\dot{r}$ is neglected, and the term $m(h-d)(\dot{v}+ur)$ is considered on the right side of 4.52, since in [7] the lateral acceleration is $a_y = \dot{v} + ur$. To make the last assumption, it is necessary to consider small angles: $\cos\phi \approx 1, \sin\phi \approx \phi$. The cross moment of inertia J_{xz} is also neglected in the yaw equilibrium. The wheel dynamics are modeled in the same way as in this work.

Similar considerations can be done for the model reported in [8], where a full vehicle model for driving simulators is illustrated. Longitudinal and lateral accelerations are considered as in the planar model, but slope and bank are considered in the external forces acting on the vehicle. Roll and pitch dynamics are equal to [7].

A different but interesting approach is reported in [9]. In fact, the derivation of EOM is carried out with Lagrange equations. The vehicle model consists of 14 DoFs: 6 for the body motions, 4 for the rotations of the wheels, and 4 for the vertical displacement of the unsprung masses. In this paper there is an interesting discussion of different reference frames adopted. The EOM are derived in a ground-fixed coordinate system. The moving reference frame is fixed on the RC and a third local reference frame is fixed on the CoG, and it is subject to pitch and roll. The pitch center is located in a different position with respect to CoG and RC. The calculation of the

kinetic energy is referred to the CoG. Its velocities are transformed from the absolute reference frame to the local one in order to compute the kinetic energy. However, the rotational velocities are considered equal in all reference systems. This is different with respect to the derivation in Chapter 9 of [3].

5 MAPs - RESULTS

5.1 General overview

The Map of Achievable Performance is a new global approach which provides a way to analyze the overall steady-state handling features of road/race cars. In fact, it is a general tool for any real car and any mathematical model. The steady-state condition is represented in a practical way by the vehicle going round along a circular path of constant radius, at a constant forward speed. In the MAP approach, there are two key concepts:

- the achievable region: given a vehicle, the totality of the achievable trim conditions are enclosed in a limited region;
- the level curves: the vehicle peculiar features are obtained for different values of a desired variable.

The two concepts are connected, in fact the achievable region can be obtained by the envelope of the level curves.
MAPs are two-dimensional illustrations of potentially any pair of vehicle related variables, that provide the reader with an at-a-glance grasp of any possible steady-state condition achievable, identified by a region in the chosen two dimensional plane [2], and the level curves add information on a third variable of interest.
As mentioned above, the core of MAPs is steady-state condition, which means that the driver imposes longitudinal velocity u and steering angle δ, and the vehicle reacts with constant lateral velocity v, constant yaw rate r, constant roll angle ϕ and constant pitch angle θ. Therefore, the steady state behavior is characterized by these 4 parameters. Moreover, the lateral velocity and the yaw rate can be normalized with respect to longitudinal velocity to obtain a more geometric description:

$$\beta = \frac{v(\delta, u)}{u} \qquad\qquad \rho = \frac{r(\delta, u)}{u} \tag{5.1}$$

with β the sideslip angle of the vehicle and ρ is a sort-of-curvature.
The input achievable regions are subject to practical limitations:

- maximum steering angle δ_{max};
- maximum vehicle speed u_{max};
- maximum lateral acceleration $a_{y,max}$, which can be seen as the achievable $u_{lim}(\delta)$ for a given steer angle due to the limited grip.

Output achievable regions are the image of input achievable regions.
Since the driver's input are (u, δ), the testing procedures are simple and widespread:

- constant speed u with slowly increasing steer angle δ;

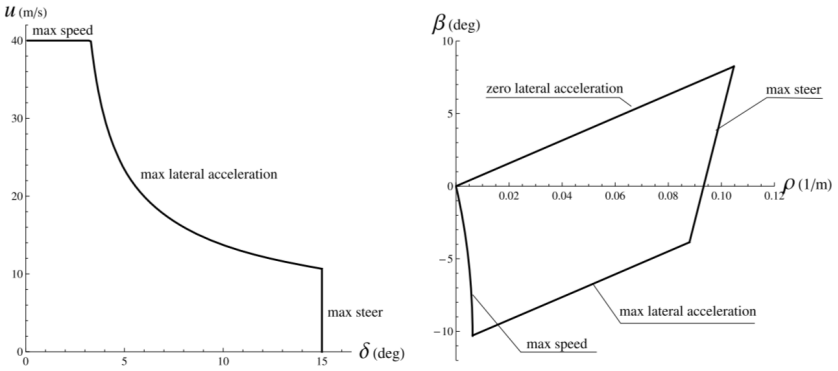

Figure 5.1: Example of achievable input region (left) and achievable output region (right) [3].

- constant steer angle δ with slowly increasing speed u.

Therefore, combining the level curves obtained with the two procedures, it is possible to obtain the output achievable region.
The building of MAPs is based on a simple idea: in Chapter 6 of [3] it is reported that "given two (feasible) constant inputs, e.g. longitudinal speed u and steer angle δ, a vehicle shall reach steady-state cornering". Thus the idea is to solve the differential equations of the model, fixing u and δ and imposing the derivatives with respect to time equal to zero. Once the solution (u, v, r, ϕ, θ) is obtained, it is possible to compute many parameters that are interesting for MAPs:

- sideslip angle: $\beta = \arctan \frac{v}{u} \approx \frac{v}{u}$
- sort of curvature: $\rho = \frac{r}{u}$
- lateral acceleration: $a_y = ur$
- longitudinal acceleration: $a_x = -vr$

It is possible to combine many pairs of these parameters to obtain the MAPs.
In the following sections several MAPs are reported. In particular, some of them are obtained both for planar and three-dimensional models, thus a comparison is carried out. Then, some MAPs are only available for the three-dimensional model since they depict the roll and pitch angles.

5.2 Constant velocity analysis

In this section, the analysis performed at constant u and slowly increasing δ is reported. The maximum steering angle is $\delta_{max} = 15\,\mathrm{deg}$, while the velocity test values are collected in the legend reported in each figure. It's important to note that the curves are trimmed at the maximum lateral acceleration achieved during the simulation, thus the final points of each curve identify the lateral acceleration limit of the MAP (and of the vehicle).

$\delta - \beta$ MAP

Since δ starts with a null value, each level curve has its origin in (0,0). Then, when the vehicle reaches its maximum achievable lateral acceleration, each level curve ends. Therefore, the first information given by the MAP is the maximum steer angle at which the vehicle obtain the maximum lateral acceleration for a given velocity: it decreases with the increase of forward speed. Then, it is noticeable the linear trend of β with δ at low speeds: in this case β is made out of a kinematic contribution only, without dynamic contribution, in fact the curves in the 3D model are almost identical to the 2D model. The differences arise for $u \geq 10m/s$, when the dynamic sideslip contribution becomes more significant. In general, it appears that, with the 3D model, the trend of β reaches a sort of saturation faster than the planar model. In addition, this MAP shows the transition between the following two vehicle configurations (Fig. 5.3):

- *nose-out*: the sideslip angle β is positive and aligned with the steer angle δ (see Fig. 3.1 for sign convention), resulting in the vehicle pointing its "nose" outside the trajectory;
- *nose-in*: the sideslip angle β is negative and opposite to the steer angle δ, resulting in the vehicle pointing its "nose" inside the trajectory.

However, it appears that the three-dimensional dynamics don't affect the transition value of δ.

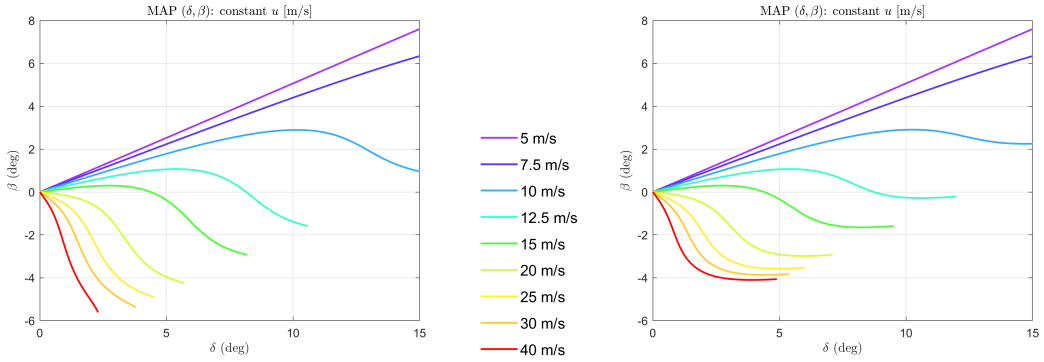

Figure 5.2: MAP $\delta - \beta$ with constant u level curves. Planar model on the left, three-dimensional model on the right.

$\delta - r$ MAP

In this MAP is noticeable the nearly linear trend of the yaw rate for slow speeds. Increasing u, the maximum yaw rate comes to a saturation, and the peak value decreases as the velocity increases. This can be explained by the lateral acceleration limit: the maximum a_y achievable in steady state is ur, therefore the limit is due to lateral friction limits. However, it seems that the three-dimensional model reaches the maximum lateral acceleration for higher value of δ, despite the peak has really similar values between the two models.

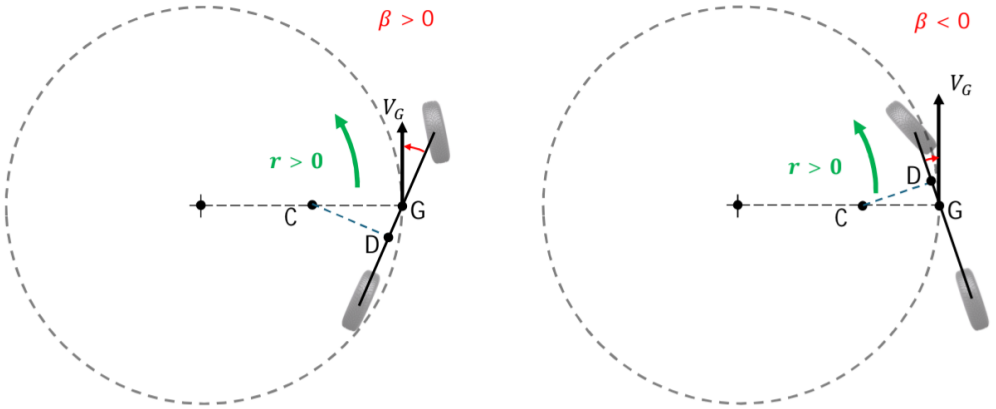

Figure 5.3: Vehicle configuration taking a left turn: *nose-out* on the left and *nose-in* on the right. Reference: Lenzo, Basilio. "Vehicle dynamics - fundamentals" in *Vehicle Dynamics, Control and Design*. Cham: Springer International Publishing, 2025.

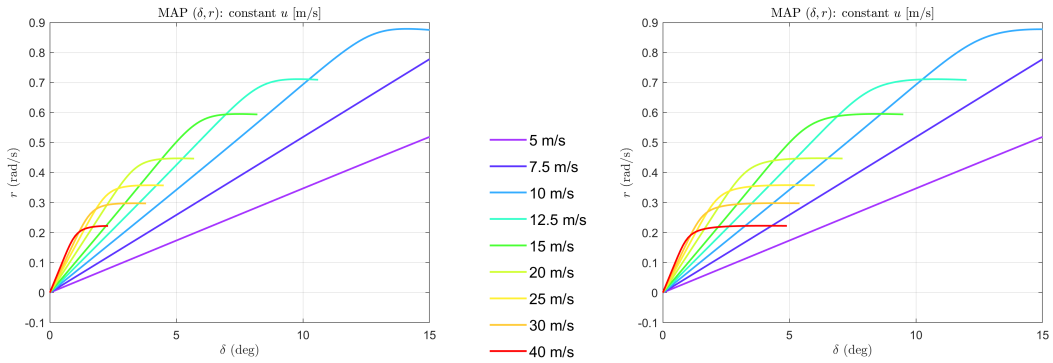

Figure 5.4: MAP $\delta - r$ with constant u level curves. Planar model on the left, three-dimensional model on the right.

$\delta - \rho$ MAP

It is useful to recall that the curves are trimmed at maximum lateral acceleration. Thus the line identified by the trim points is the maximum a_y limit. This MAP clearly shows the amount of steering angle available to increase the maximum value of ρ, which decreases as the speed increases. Since ρ is the yaw rate normalized with respect to u, it is also noticeable in this MAP that the maximum value of a_y is obtained for higher steering angles in the 3D model, despite the peak is really similar. Focusing on the three-dimensional model, it is clearly an understeering vehicle: the driver could increase the steering angle, without an increase of ρ.

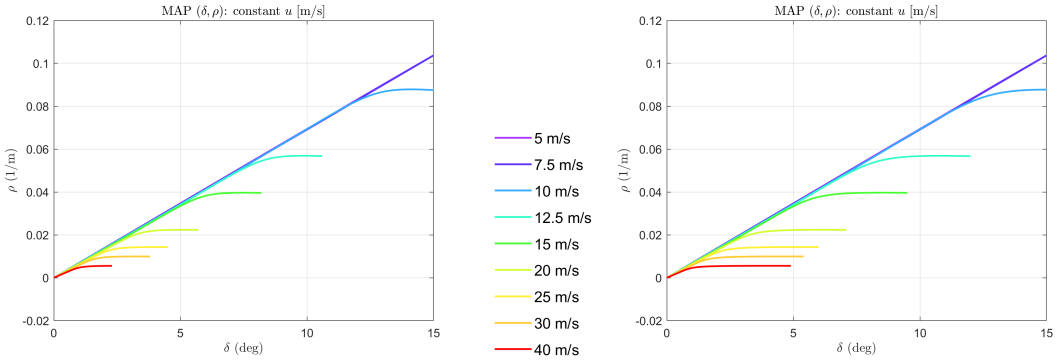

Figure 5.5: MAP $\delta - \rho$ with constant u level curves. Planar model on the left, three-dimensional model on the right.

$\rho - \beta$ MAP

This MAP is an example of output region: both axes represent an output value. The achievable region is smaller in the three-dimensional model:

- at low speeds, the sideslip angle β is positive at the lateral acceleration limit (nose-out configuration), and, considering the 10 m/s curve, it has a lower value in the planar model;
- at high speeds, the sideslip angle β is negative at the lateral acceleration limit (nose-in configuration) and its absolute value is smaller in the three-dimensional model.

These considerations yield a bigger output achievable region for the planar model, thus the roll and pitch dynamics reduce the achievable set of equilibrium points. In Section 5.5 the direct comparison is illustrated.

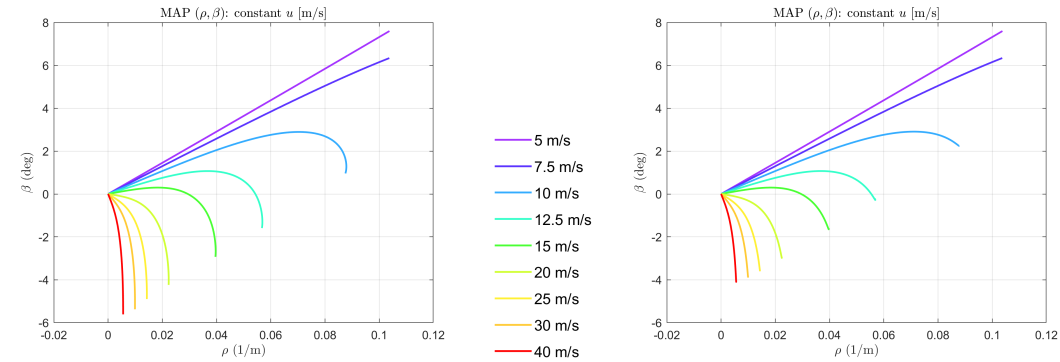

Figure 5.6: MAP $\rho - \beta$ with constant u level curves. Planar model on the left, three-dimensional model on the right.

$a_y - \beta$ MAP

Also in this case the MAP consists of two output parameters. The considerations made in the previous paragraph are visually explained here. It is clear that the maximum a_y limit is narrower for the three-dimensional model. The peak value of a_y is similar between the two models ($\approx 9m/s^2$), but it is obtained for smaller absolute values of β at high speeds and for similar values at low speeds.

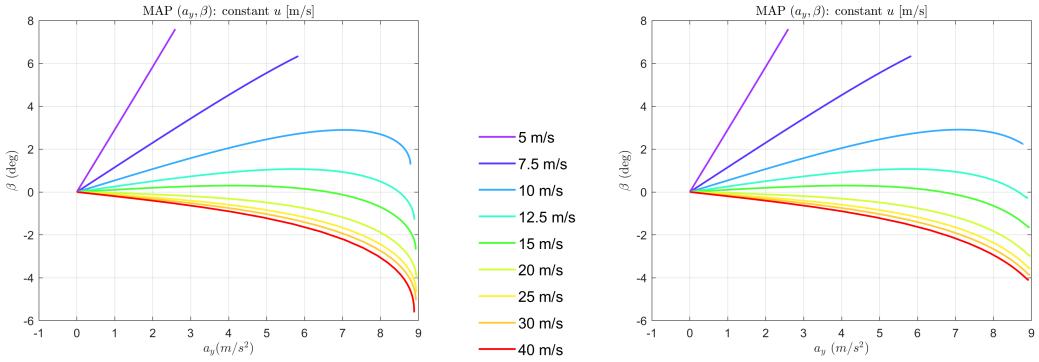

Figure 5.7: MAP $a_y - \beta$ with constant u level curves. Planar model on the left, three-dimensional model on the right.

5.3 Constant steering angle analysis

In this section, the analysis performed at constant δ and slowly increasing u is reported. The velocity span is from 5 m/s to 40 m/s, while the steering angle test values are collected in the legend reported in each figure. Also in this case the curves are trimmed at the maximum achievable lateral acceleration.

$u - \beta$ MAP

It is useful to focus on this MAP together with the $\delta - \beta$ MAP reported in Fig. 5.2. An additional information that can be retrieved in this MAP is the transition speed at which $\beta = 0$: it is noticeable that transition speed decreases as δ increases. In addition, it is noticeable that the maximum lateral acceleration is achieved exclusively with the nose-out configuration for $\delta > 12\,\mathrm{deg}$: in fact, for high values of the steering angle, the grip limit is reached at low speeds. It is possible to reaffirm that the peak of a_y is reached for higher speeds and lower absolute values of β in the three-dimensional model.

$u - r$ MAP

In this MAP similar considerations to the $\delta - r$ MAP can be done. There is a noticeable linear trend for low speeds and saturation of the yaw rate: however, the maximum lateral acceleration

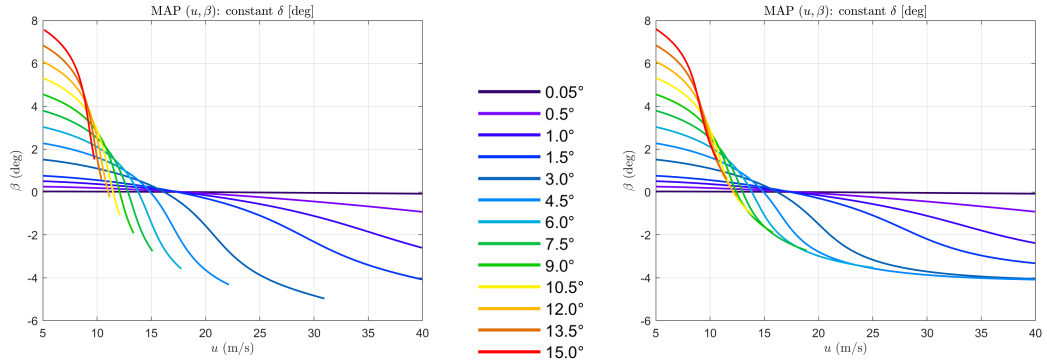

Figure 5.8: MAP $u - \beta$ with constant δ level curves. Planar model on the left, three-dimensional model on the right.

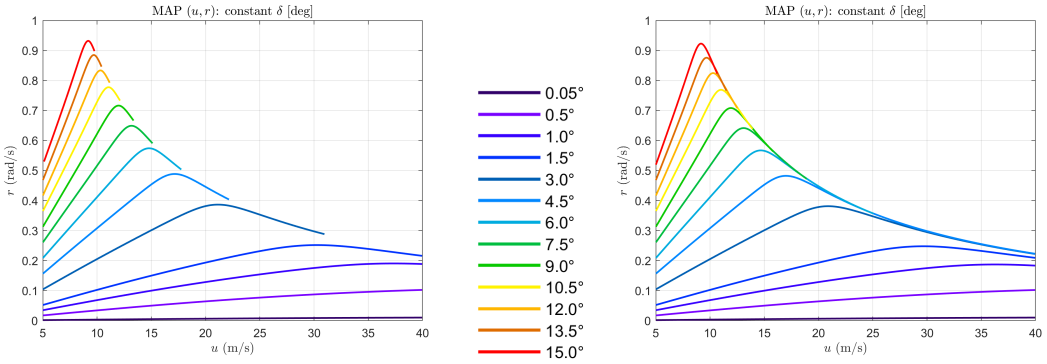

Figure 5.9: MAP $u - r$ with constant δ level curves. Planar model on the left, three-dimensional model on the right.

ur is not achieved at the maximum yaw rate. The two models produce really similar results.

Other MAPs

In the following page, several MAPs for constant δ analysis are reported. To get more insights, it is useful to focus on *coupled* MAPs, i.e. maps that share the same y-axis but with different analysis. For example, Fig. 5.2 with Fig. 5.8, Fig. 5.4 with Fig. 5.9, Fig. 5.5 with Fig. 5.10.
The output region MAPs will be useful in 5.5 combining the constant u analysis and the constant δ analysis in the same plot.

5.4 Roll-related and pitch-related MAPs

In this section, all-new MAPs are illustrated. In fact, the plots containing information on roll angle ϕ and pitch angle θ appear for the first time.
Starting from the simplest insight, the linear dependences $\phi - a_y$ and $\theta - a_x$ are verified. The

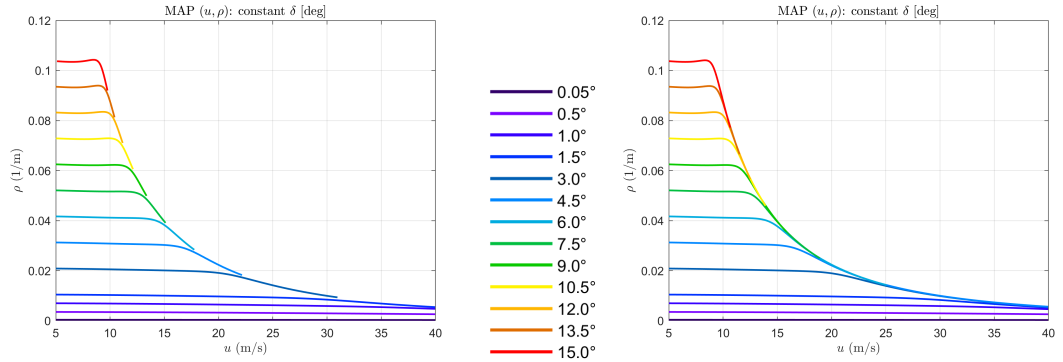

Figure 5.10: MAP $u - \rho$ with constant δ level curves. Planar model on the left, three-dimensional model on the right.

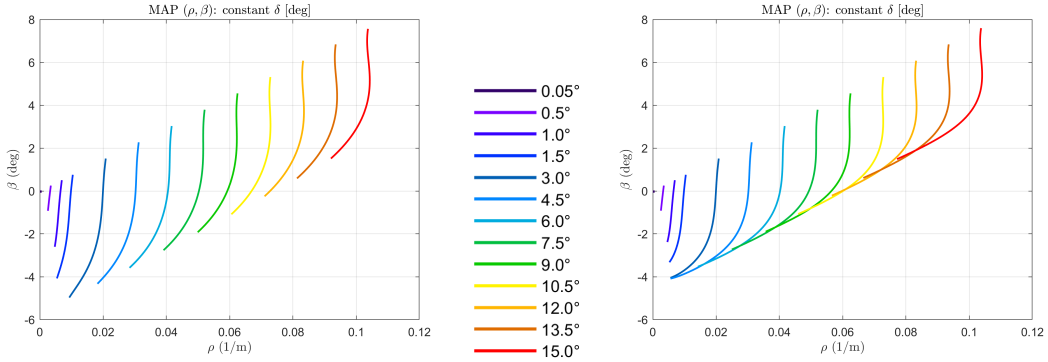

Figure 5.11: MAP $\rho - \beta$ with constant δ level curves. Planar model on the left, three-dimensional model on the right.

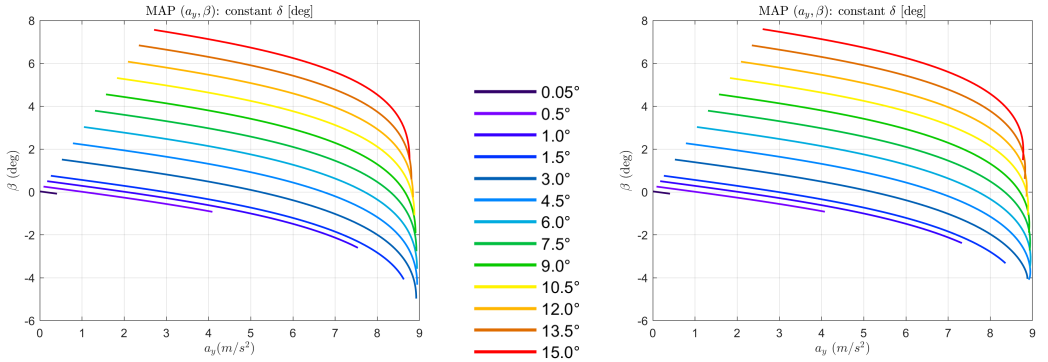

Figure 5.12: MAP $a_y - \beta$ with constant δ level curves. Planar model on the left, three-dimensional model on the right.

plots are not reported due to its simple form, i.e. a line, in both analyses. It is possible to compute the slope from the EOM, remembering that at steady state the time derivatives are null. Thus, considering the third and fourth equations of 4.45 and the moments expressed as in 4.13 and 4.14, at steady state the left-hand side is null, and the roll and pitch velocities too. Thus the result is:

$$L_{G'} = 0 \rightarrow -k_\phi \phi + ma_y(h-d) + mg(h-d)\phi = 0 \rightarrow \frac{\phi}{a_y} = \frac{m(h-d)}{k_\phi - mg(h-d)} \tag{5.2}$$

$$M_{G'} = 0 \rightarrow -k_\theta \theta - ma_x(h-d) + mg(h-d)\theta = 0 \rightarrow \frac{\theta}{a_x} = \frac{-m(h-d)}{k_\theta - mg(h-d)} \tag{5.3}$$

It could be useful to illustrate the two following MAPs: $\delta - \phi$ together with $\delta - a_y$ at constant u level curves.

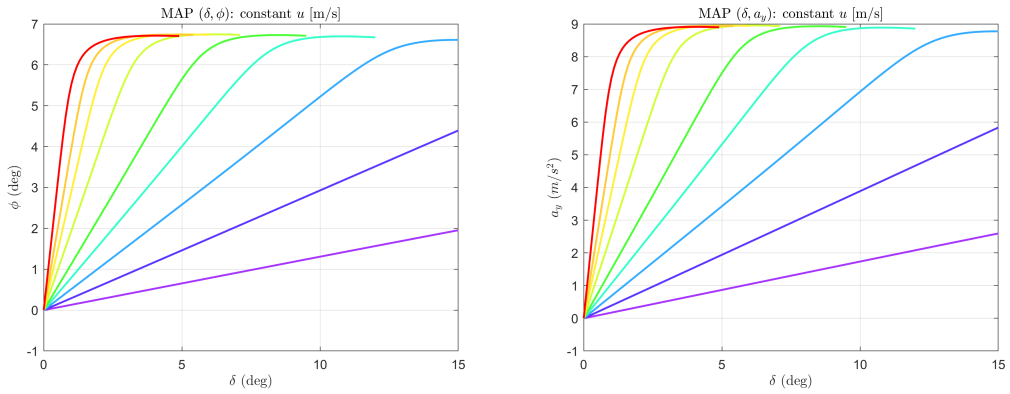

Figure 5.13: MAPs $\delta - \phi$ on the left, and $\delta - a_y$ on the right.

It's clear that the trend is exactly the same for both the parameters. The saturation occurs at lower values of δ as u increases.
The roll angle is related in an interesting way with ρ. On the left-hand side of Fig. 5.14 the linear trend between the two parameters is clearly seen: at high speeds the increasing δ leads to high roll angles for small curvatures, reaching the maximum a_y for smaller values of ρ with respect to low speeds. Considering the right-hand side of Fig. 5.14, the maximum a_y limit is clearly defined. The increasing u leads to increasing value of ϕ despite an initial almost constant value of ρ. Then, when the friction limit is reached, the curvature decreases until the lateral acceleration limit is reached.
Combining the two MAPs, the output achievable region is obtained, and it will be shown in Section 5.5.
To better understand the right-hand side MAP of 5.14, the MAP $u - \phi$ is illustrated. In this case, the trend is not linear, even at low speeds and small values of δ.
In the whole set of ϕ-related MAPs, the roll angle is always positive, which is consistent with the axis convention used, since the car is taking a left turn. This result is expected; in fact, ϕ cannot be negative. Thus, the analysis of additional MAPs would lead to similar considerations already done.

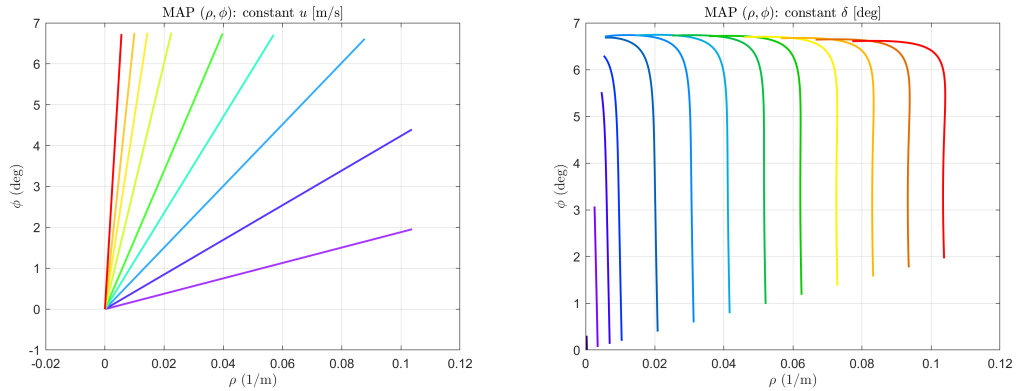

Figure 5.14: MAPs $\rho - \phi$, constant u level curves on the left, constant δ level curves on the right. The values of u and δ increase from purple to red.

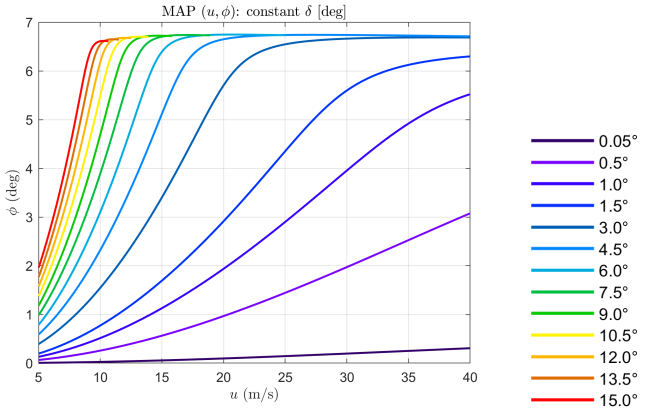

Figure 5.15: MAP $u - \phi$ with constant δ level curves.

On the other hand, the pitch angle behaviour is more interesting: it can assume both positive and negative values, and an interesting insight will be presented in the following pages. The axis convention implies $\theta > 0$ under braking (negative a_x) and $\theta < 0$ under traction (positive a_x). The first interesting MAP is the $\delta - \theta$ one (Fig. 5.16). The first feature to note is the non-linear trend. Then, it is noticeable that $\theta > 0$ for low speeds and $\theta < 0$ for high speeds. At medium speeds, there is a transition from positive values to negative ones as δ increases. To explain this behavior, it is useful to remember the linear dependence between θ and a_x (Eq. 5.3): it has negative sign, and this is consistent with the convention explained above. Therefore, the MAP $\delta - a_x$ is the same as $\delta - \theta$, but mirrored with respect to x-axis: the longitudinal acceleration changes its sign also. At steady state, $a_x = -vr$, and, as reported in the previous pages, it is clear that the yaw rate r is always positive; on the other hand, the lateral velocity v can be positive or negative, and it can be seen in β-related MAPs. Therefore, the transition from positive to negative values of θ is due to the sideslip angle β: the nose-in or nose-out configurations affect

the pitch angle. This is an interesting result, and a visual representation is in the $\beta - \theta$ MAP (Fig. 5.17): the transition point for each curve is located in the origin. It is clear that for nose-out configuration ($\beta > 0$) the longitudinal acceleration is negative, and the pitch angle is positive; for nose-in configuration ($\beta < 0$) the longitudinal acceleration is positive, and the pitch angle is negative.

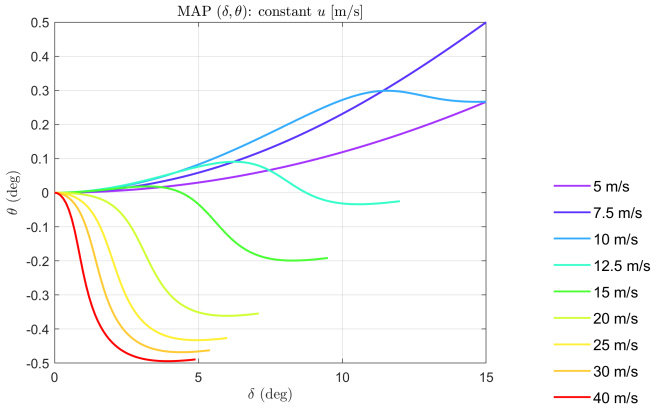

Figure 5.16: MAP $\delta - \theta$ with constant u level curves.

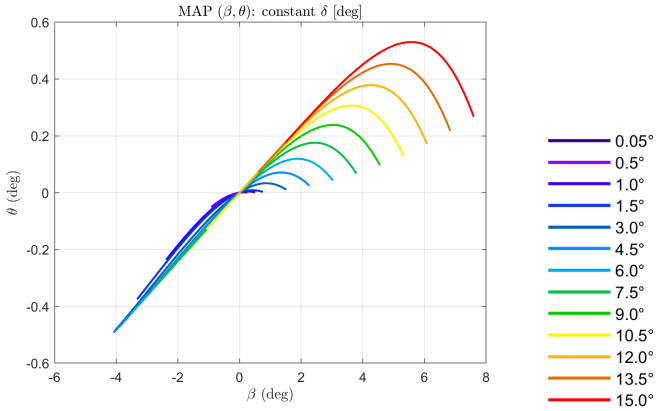

Figure 5.17: MAP $\beta - \theta$ with constant u level curves.

Considering the $u - \theta$ MAP, the transition speed between positive and negative values of θ is the same of the transition speed for β, which can be seen in Fig. 5.8. To deepen this insight, the MAPs $a_y - \theta$ are reported.

5.5 Output achievable regions

In this section, some output achievable regions are illustrated. Firstly, two regions are compared between the planar model and the 3D model. Then, two regions related to roll and pitch are

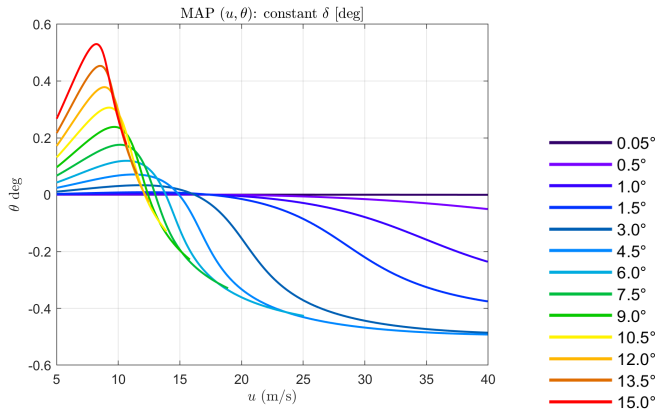

Figure 5.18: MAP $u - \theta$ with constant u level curves.

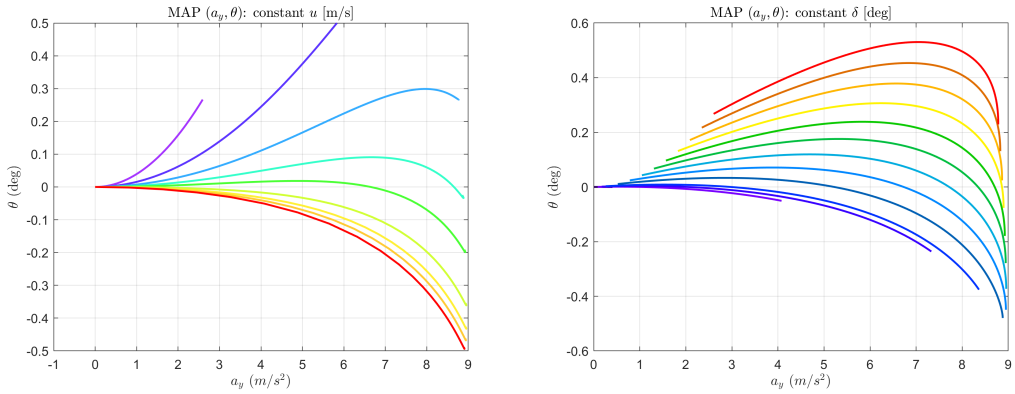

Figure 5.19: MAPs $a_y - \theta$, constant u level curves on the left, constant δ level curves on the right. The values of u and δ increase from purple to red.

illustrated.
The first output achievable region is identified by the parameters ρ, β (Fig. 5.20). The upper limit, which is determined by the minimum velocity, is identical between the two models, recalling that at low speeds the kinematic contributes to β is dominant. Moving to the lower limit, which is determined by the lateral acceleration limit, it is noticeable that the planar model has a bigger achievable region (mind the y-axis scale). Therefore, the three-dimensional model, which includes roll and pitch motions, is affected by dynamic contributes more than the planar model. It is possible to say that the sprung mass movements reduce the total set of equilibrium points achievable by the vehicle.

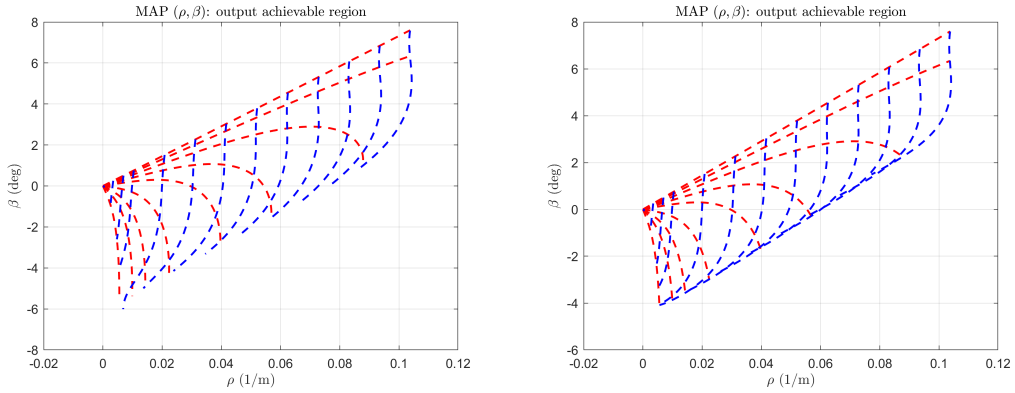

Figure 5.20: Output achievable region in $\rho - \beta$ MAP. On the left the planar model, on the right the 3D model.

The second region is identified by the parameters a_y, β (Fig. 5.21). The considerations made for the sideslip angle can be reiterated. However, it's useful to point out that the peak value of a_y is not affected by the three-dimensional dynamics: in both model the maximum value is $\approx 9\, m/s^2$. It seems that the relation between pitch angle and sideslip angle could affect the maximum amount of nose-in configuration of the vehicle.
Considering the roll and pitch related MAPs, two regions are illustrated.

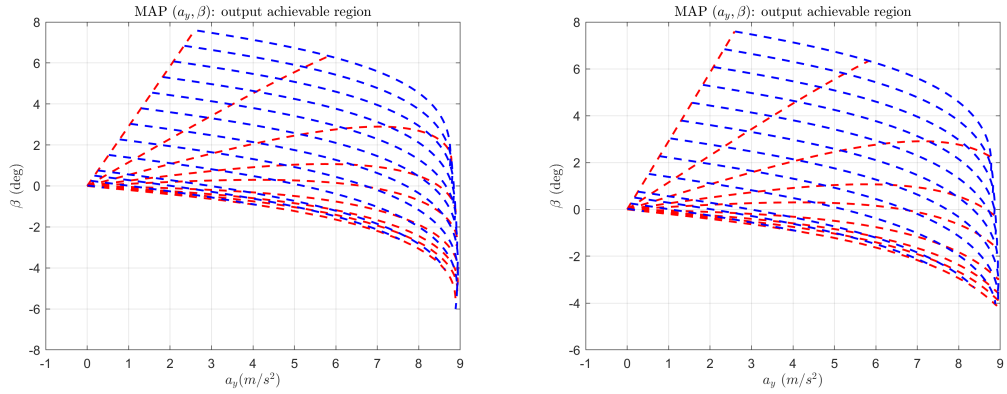

Figure 5.21: Output achievable region in $a_y - \beta$ MAP. On the left the planar model, on the right the 3D model.

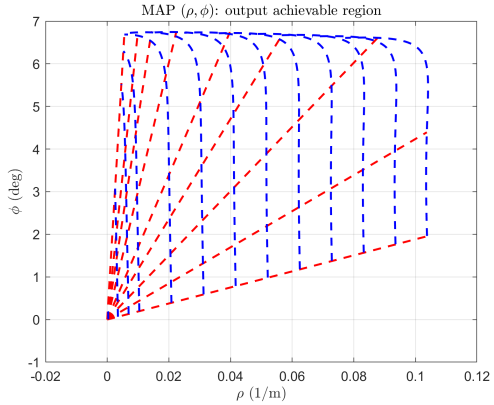

Figure 5.22: Output achievable region in $\rho - \phi$ MAP.

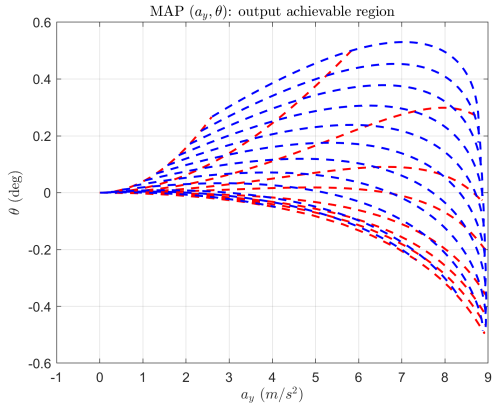

Figure 5.23: Output achievable region in $a_y - \theta$ MAP.

6 Conclusions

In this thesis, the development of a three-dimensional vehicle model has been presented. It is a double track model including roll and pitch dynamics, and wheel dynamics also. Its peculiar features are represented by a state-space formulation, where the load transfers are treated as state variables. A new formulation of longitudinal load transfer has been proposed: it can be employed in transient conditions and is affected by pitch stiffness and damping. A PI controller has been implemented to assign the correct torque value to the driving wheels. The model has been implemented to study the Maps of Achievable Performance (MAPs), which are 2D representations of related parameters which define the vehicle handling at steady state. The simulations include standard manoeuvres, such as fixed forward velocity with slowly increasing steering angle, and fixed steering angle with slowly increasing forward velocity. A comparison between the output achievable regions for planar and three-dimensional model has been carried out, resulting in a smaller region for the latter. Therefore, the spatial dynamics affects the handling of the vehicle reducing the achievable performance. Then, *advanced* MAPs have been presented for the first time: they illustrate roll and pitch angles related to the other handling parameters. The results showed their linear dependencies with lateral and longitudinal acceleration. Then, the MAPs involving the roll angle showed an expected behavior: it is always positive taking a left turn, and it doesn't assume negative sign. On the other hand, the MAPs involving the pitch angle showed an interesting behavior: in fact, pitch angle and sideslip angle are related. For zero sideslip, the pitch is zero. For a nose-out configuration, i.e. positive sideslip, the pitch angle is positive, i.e. the longitudinal acceleration is negative and the car experiences the movement that is typical under braking. For a nose-in configuration, i.e. negative sideslip, the pitch angle is negative, i.e. the longitudinal acceleration is positive and the car experiences the movement that is typical under traction. Focusing on different MAPs at the same time, it is possible to retrieve the transition speed, the transition steering angle, the peak of lateral acceleration and many more handling features of the vehicle.

Future developments could be the extension of the model's degrees of freedom: in particular, the vertical displacement of the sprung mass (*heave*) and unsprung masses (*wheel hop*) could be implemented. The equations of motion would change a little due to the distinction between sprung and unsprung masses, and it would be interesting to find out the differences in handling features.

An other interesting future development is the study of *Handling Bricks* ([3], Chapters 7-8): they represent a link between the steady state MAPs and the handling features under transient conditions. So far they have been studied for planar models, and it would be interesting to extend them to a spatial model, including some bricks dependent on roll and pitch dynamics.

BIBLIOGRAPHY

[1] W. H. Organization, *Global status report on road safety 2023*. 2023.

[2] M. Guiggiani and B. Lenzo, "Maps of achievable performance: a new general tool for vehicle handling analysis," *The IAVSD International Symposium on Dynamics of Vehicles on Roads and Tracks*, 2023.

[3] M. Guiggiani, *The Science of Vehicle Dynamics - Handling, Braking, and Ride of Road and Race cars*. Springer, 3rd ed., 2023.

[4] G. Righetti, A. Sassella, and B. Lenzo, "A gradient descent-based vehicle optimizator for enhanced state estimation," *IFAC-PapersOnLine*, vol. 59, no. 5, pp. 211–216, 2025. 11th IFAC Symposium on Advances in Automotive Control AAC 2025.

[5] M. Bruschetta, E. Picotti, E. Mion, Y. Chen, A. Beghi, and D. Minen, "A nonlinear model predictive control based on virtual driver for high performance driving," *2019 IEEE Conference on Control Technology and Applications (CCTA)*, 2019.

[6] K. Berntorp, "Derivation of a six degrees-of-freedom ground-vehicle model for automotive applications," 2013.

[7] J. D. Setiawan, M. Safarudin, and A. Singh, "Modeling, simulation and validation of 14 dof full vehicle model," *International Conference on Instrumentation, Communication, Information Technology, and Biomedical Engineering 2009*, 2009.

[8] J. G. Fernandez, *A Vehicle Dynamics Model for Driving Simulators*. PhD thesis, Chalmers University of Technology, 2012.

[9] F. Cheli, E. Leo, S. Melzi, and F. Mancosu, "A 14 dof model for the evaluation of vehicle's dynamics: numerical-experimental comparison," *International Journal of Mechanics and Control*, vol. 06, no. 02, 2005.